ELSEVIER

Journal of Quantitative Spectroscopy & Radiative Transfer 102 (2006) 316–342

Journal of Quantitative Spectroscopy & Radiative Transfer

www.elsevier.com/locate/jqsrt

VLIDORT: A linearized pseudo-spherical vector discrete ordinate radiative transfer code for forward model and retrieval studies in multilayer multiple scattering media

Robert J.D. Spurr*

RT Solutions, Inc., 9 Channing Street, Cambridge, MA 02138, USA

Received 19 April 2006; received in revised form 6 May 2006; accepted 6 May 2006

Abstract

We describe a new vector discrete ordinate radiative transfer model with a full linearization facility. The VLIDORT model is designed to generate simultaneous output of Stokes vector light fields and their derivatives with respect to any atmospheric or surface property. We develop new implementations for the linearization of the vector radiative transfer solutions, and go on to show that the complete vector discrete ordinate solution is analytically differentiable for a stratified multilayer multiply scattering atmospheric medium. VLIDORT will generate all output at arbitrary viewing geometry and optical depth. The model has the ability to deal with attenuation of solar and line-of-sight paths in a curved atmosphere, and includes an exact treatment of the single scatter computation. VLIDORT also contains a linearized treatment for non-Lambertian surfaces. A number of performance enhancements have been implemented, including a facility for multiple solar zenith angle output. The model has been benchmarked against established results in the literature.

Keywords: Radiative transfer; Polarization; Linearization; Discrete ordinates; Pseudo-spherical

1. Introduction

The modern treatment of the equations of radiative transfer (RT) for polarized light dates back to the pioneering work by Chandrasekhar in the 1940s [1]. Using a formulation in terms of the Stokes vector for polarized light, Chandrasekhar was able to solve completely the polarization problem for an atmosphere with Rayleigh scattering, and benchmark calculations from the 1950s are still appropriate today [2]. In the early 1970s, general formulations of the scattering matrices for polarized light were developed independently by several authors [3–5]. In the early 1980s, Siewert reformulated the Legendre function development of the scattering matrix for polarized light in a convenient analytic manner [6–8], and most vector RT models now follow this formulation. Garcia and Siewert developed complete vector RT solutions for the slab problem using the spherical harmonics method [9] and the F_N method [10], and generated two sets of benchmark results for this problem. Also in the 1980s, a group in the Netherlands carried out some parallel developments.

*Corresponding author. Tel.: +1 617 492 1183; fax: +1 617 354 3415.
E-mail address: rtsolutions@verizon.net.

0022-4073/$ - see front matter © 2006 Elsevier Ltd. All rights reserved.
doi:10.1016/j.jqsrt.2006.05.005

Following detailed mathematical studies of polarized RT [11,12], a doubling-adding (interaction principle) model was developed for atmospheric RT modeling [13,14]. This group also provided benchmark results for the slab problem [15].

The well-known DISORT discrete ordinate model developed by Stamnes and co-workers was released in 1988 for general use in plane-parallel multilayer multiple scattering media [16]. A vector discrete ordinate model VDISORT was developed in the 1990s [17]. In two papers appearing in 2000, Siewert revisited the slab problem from a discrete ordinate viewpoint, and derived new solutions for the scalar [18] and vector [19] radiative transfer equations (RTEs). These solutions used Green's functions for the generation of particular solutions for the solar scattering term [20]. For the vector RTE, this analysis showed that complex eigensolutions for the homogeneous equations are important [19]. Siewert also provided a new set of benchmark results; this set and the results from [10] provide standards for validation in the present work.

In the last decade, there has been increasing recognition of the need for RT models to generate fields of analytic radiance derivatives (Jacobians) with respect to atmospheric and surface variables, in addition to simulated radiances. Such "linearized" models are extremely useful in classic inverse problem retrievals involving iterative least-squares minimization (with and without regularization) [21]. At each iteration step, the simulated radiation field is expanded in a Taylor series about the given state of the atmosphere-surface system. Only the linear term in this expansion is retained, and this requires partial derivatives of the simulated radiance with respect to atmospheric and surface parameters that make up the state vector of retrieval elements and the vector of assumed model parameters that are not retrieved but are sources of error in the retrieval. A number of "linearized" RT models have been developed in recent years [22–28].

In this paper, we describe a new linearized vector code VLIDORT that is an addition to the family of LIDORT (linearized discrete ordinate radiative transfer) RT codes [28–32]. The original LIDORT code [28] generated Jacobians and radiances for the top of atmosphere (TOA) reflectance scenario for a plane-parallel multilayer atmosphere. This was generalized to include a pseudo-spherical treatment of solar beam attenuation, output at arbitrary optical thickness and viewing geometry, the use of Green's function solution methods, and the development of an exact single scatter correction [29,30]. There is also a sphericity correction for wide-angle off-nadir viewing in a curved atmosphere [31], and a detailed treatment of Jacobians with respect to properties characterizing non-Lambertian surface reflectance functions [32].

It is well known that the use of scalar radiative transfer (neglecting polarization) can lead to considerable errors for modeling backscatter spectra in the UV [33–35]. Studies with atmospheric chemistry instruments such as GOME, SCIAMACHY and OMI have shown that the treatment of polarization is critical for the successful retrieval of ozone profiles from UV backscatter [36,37]. The role of polarization has been investigated for retrieval scenarios involving important backscatter regions such as the oxygen A-band [38–40]. It has also been demonstrated that the use of passive sensing instruments with polarization capabilities can greatly enhance retrievals of aerosol information in the atmosphere [41,42]; this is becoming a very important issue as the scientific community tries to understand the effects of aerosol forcing [43,44]. Satellite instruments such as GOME-2 (due for launch in June 2006) [45] and OCO (Orbital Carbon Observatory, launch September 2008) [46] are polarizing spectrometers; vector radiative transfer is an essential ingredient of the forward modeling component of their retrieval algorithms. Vector RT modeling is slower than its scalar counterpart, and the treatment of polarization in forward modeling has often involved the creation of look-up tables of "polarization corrections" to total intensity. However, with the advent of new and planned instruments measuring polarization, there is a need for linearized vector models to deal directly with retrieval issues.

For VLIDORT, we have extended Siewert's rigorous solution for the plane-parallel slab problem [19] to multilayer stratified media, and we have developed pseudo-spherical formulations to deal with beam attenuations in a curved atmosphere. As with the scalar code, VLIDORT has an exact single scatter correction and a treatment of non-Lambertian (BRDF) surfaces. The major new aspect of the present work is the development of the *linearization facility* for VLIDORT for the generation of analytic weighting functions. This involves the complete differentiation of the polarized RT scattering theory in a multilayer atmosphere. In general, VLIDORT linearization follows the methodology developed for the scalar LIDORT code, though there are some notable differences in the treatment of the homogeneous solutions of the vector RTE.

The paper is organized as follows. Section 2 summarizes the theoretical framework of the vector RTE, including separation of the azimuthal dependence. Section 3 contains a description of the discrete ordinate solutions of the vector RTE for the homogeneous field and the particular integral in the presence of solar source terms; this section contains a detailed treatment of the analytic derivatives of these solutions. Section 4 deals with post-processing of the vector RT: the boundary value problem in a multilayer atmosphere and output at arbitrary viewing directions. Section 5 considers other aspects of the model, including the BRDF treatment, and exact single scatter calculations to improve accuracy. In Section 6, we discuss aspects the VLIDORT software package, including benchmarking the code and preparation of optical property inputs.

2. Theoretical framework

2.1. The vector RTE

A first-principles derivation of the vector RTE has been given in the analysis of Mishchenko [47]. The basic vector RTE is

$$\mu \frac{\partial}{\partial x}\mathbf{I}(x,\mu,\phi) = \mathbf{I}(x,\mu,\phi) - \mathbf{J}(x,\mu,\phi). \tag{1}$$

Here, x is the optical thickness measured from the top of the layer, μ is the polar angle cosine measured from the upward vertical, and ϕ is the azimuth angle relative to some fixed direction. The 4-vector $\mathbf{I}$ is the diffuse field of Stokes components $\{I, Q, U, V\}$ [1], with I the total intensity, Q and U describing linearly polarized radiation, and V characterizing circularly polarized radiation. Vector $\mathbf{I}$ is defined with respect to a reference plane (usually, the local meridian plane). The degree of polarization P of the radiation is

$$P = I^{-1}\sqrt{Q^2 + U^2 + V^2}. \tag{2}$$

The vector source term $\mathbf{J}(x,\mu,\phi)$ has the form:

$$\mathbf{J}(x,\mu,\phi) = \frac{\omega(x)}{4\pi}\int_{-1}^{1}\int_{0}^{2\pi}\mathbf{\Pi}(x,\mu,\mu',\phi-\phi')\mathbf{I}(x,\mu',\phi')\,\mathrm{d}\phi'\,\mathrm{d}\mu' + \mathbf{Q}(x,\mu,\phi). \tag{3}$$

Here, ω is the single scattering albedo and $\mathbf{\Pi}$ the phase matrix for scattering. The first term in Eq. (3) represents multiple scattering contributions. For scattering of the attenuated solar beam, the inhomogeneous source term $\mathbf{Q}(x,\mu,\phi)$ is written:

$$\mathbf{Q}(x,\mu,\varphi) = \frac{\omega(x)}{4\pi}\mathbf{\Pi}(x,\mu,-\mu_0,\varphi-\varphi_0)\mathbf{I}_0\,T_a\exp[-\lambda x]. \tag{4}$$

Here, $-\mu_0$ is the cosine of the solar zenith angle (with respect to the upward vertical); ϕ_0 is the solar azimuth angle and $\mathbf{I}_0$ the Stokes vector of the incoming solar beam before attenuation.

The pseudo-spherical (P-S) beam attenuation in Eq. (4) is written $T_a\exp[-\lambda x]$, where T_a is the transmittance to the top of the layer, and λ is a geometrical factor (the "average secant"). In the P-S formulation, all scattering takes place in a plane-parallel medium, but the solar beam attenuation is treated for a curved atmosphere. For plane-parallel attenuation, we have $\lambda = -1/\mu_0$. It has been shown that the P-S approximation is accurate for solar zenith angles up to 90° [48]. Details on the pseudo-spherical formulation are found in Appendix A.

In this paper, we consider an atmosphere illuminated by natural (unpolarized) sunlight, so that the solar irradiance at TOA is given by Stokes vector $\mathbf{I}_0 = \{I_0,0,0,0\}$. We assume that the medium comprises a stratification of optically uniform layers; for each layer, the single scattering albedo ω and the phase matrix $\mathbf{\Pi}$ in Eq. (3) do not depend on the optical thickness x, and we henceforth drop this dependence.

Matrix $\mathbf{\Pi}$ relates scattering and incident Stokes vectors defined with respect to the meridian plane. The equivalent matrix for Stokes vectors with respect to the *scattering* plane is the scattering matrix $\mathbf{F}$. In this work, we restrict ourselves to scattering for a medium that is "macroscopically isotropic and symmetric" [49], with scattering for ensembles of randomly oriented particles having at least one plane of symmetry. In this case, $\mathbf{F}$ depends only on the scattering angle Θ between scattered and incident beams. Matrix $\mathbf{\Pi}$ is related to

$\mathbf{F}(\Theta)$ through application of two rotation matrices $\mathbf{L}(\pi-\sigma_2)$ and $\mathbf{L}(-\sigma_1)$ (for definitions of these matrices and the angles of rotation σ_1 and σ_2, see [48]):

$$\mathbf{\Pi}(\mu,\phi,\mu',\phi') = \mathbf{L}(\pi-\sigma_2)\mathbf{F}(\Theta)\mathbf{L}(-\sigma_1), \tag{5}$$

$$\cos\Theta = \mu\mu' + \sqrt{1-\mu^2}\sqrt{1-\mu'^2}\cos(\phi-\phi'). \tag{6}$$

In our case, $\mathbf{F}(\Theta)$ has the well-known form:

$$\mathbf{F}(\Theta) = \begin{pmatrix} a_1(\Theta) & b_1(\Theta) & 0 & 0 \\ b_1(\Theta) & a_2(\Theta) & 0 & 0 \\ 0 & 0 & a_3(\Theta) & b_2(\Theta) \\ 0 & 0 & -b_2(\Theta) & a_4(\Theta) \end{pmatrix}. \tag{7}$$

The upper left entry in this matrix is the phase function and satisfies the normalization condition:

$$\frac{1}{2}\int_0^\pi a_1(\Theta)\sin\Theta\,\mathrm{d}\Theta = 1. \tag{8}$$

2.2. Azimuthal separation

For the special form of $\mathbf{F}$ in Eq. (7), the dependence on scattering angle allows us to develop expansions of the six independent scattering functions in terms of a set of generalized spherical functions $P^l_{mn}(\cos\Theta)$ [49]:

$$a_1(\Theta) = \sum_{l=0}^{LM}\beta_l P^l_{00}(\cos\Theta), \tag{9}$$

$$a_2(\Theta) + a_3(\Theta) = \sum_{l=0}^{LM}(\alpha_l+\zeta_l)P^l_{2,2}(\cos\Theta), \tag{10}$$

$$a_2(\Theta) - a_3(\Theta) = \sum_{l=0}^{LM}(\alpha_l-\zeta_l)P^l_{2,-2}(\cos\Theta), \tag{11}$$

$$a_4(\Theta) = \sum_{l=0}^{LM}\delta_l P^l_{00}(\cos\Theta), \tag{12}$$

$$b_1(\Theta) = \sum_{l=0}^{LM}\gamma_l P^l_{02}(\cos\Theta), \tag{13}$$

$$b_2(\Theta) = -\sum_{l=0}^{LM}\varepsilon_l P^l_{02}(\cos\Theta). \tag{14}$$

The six sets of "Greek constants" $\{\alpha_1, \beta_1, \gamma_1, \delta_1, \varepsilon_1, \zeta_1\}$ must be specified for each moment l in these spherical-function expansions. The number of terms LM depends on the level of numerical accuracy. Values $\{\beta_1\}$ are the phase function Legendre expansion coefficients as used in the scalar RTE. These "Greek constants" are commonly used to specify the polarized-light single-scattering law, and there are a number of efficient analytical techniques for their computation, not only for spherical particles (see for example [12]) but also for randomly oriented homogeneous and inhomogeneous non-spherical particles and aggregated scatterers [50–52].

With this representation in Eqs. (9)–(14), one can then develop a Fourier decomposition of $\mathbf{\Pi}$ to separate the azimuthal dependence (cosine and sine series in the relative azimuth $\phi-\phi_0$). The same separation is applied to the Stokes vector itself. A convenient formalism for this separation was developed by Siewert and co-workers [6–8], and we summarize the results here for illumination by natural light. The Stokes vector Fourier decomposition is

$$\mathbf{I}(x,\mu,\phi)=\frac{1}{2}\sum_{l=m}^{LM}(2-\delta_{m,0})\mathbf{\Phi}^m(\phi-\phi_0)\mathbf{I}^m(x,\mu), \tag{15}$$

$$\mathbf{\Phi}^m(\phi)=diag\{\cos m\phi,\cos m\phi,\sin m\phi,\sin m\phi\}. \tag{16}$$

The phase matrix decomposition is:

$$\mathbf{\Pi}(\mu,\phi,\mu',\phi')=\frac{1}{2}\sum_{l=m}^{LM}(2-\delta_{m,0})\left[\mathbf{C}^m(\mu,\mu')\cos m(\phi-\phi')+\mathbf{S}^m(\mu,\mu')\sin m(\phi-\phi')\right], \tag{17}$$

$$\mathbf{C}^m(\mu,\mu')=\mathbf{A}^m(\mu,\mu')+\mathbf{D}\mathbf{A}^m(\mu,\mu')\mathbf{D}, \tag{18}$$

$$\mathbf{S}^m(\mu,\mu')=\mathbf{A}^m(\mu,\mu')\mathbf{D}-\mathbf{D}\mathbf{A}^m(\mu,\mu'), \tag{19}$$

$$A^m(\mu,\mu')=\sum_{l=m}^{LM}\mathbf{P}_l^m(\mu)\mathbf{B}_l\mathbf{P}_l^m(\mu'), \tag{20}$$

$$\mathbf{D}=diag\{1,1,-1,-1\}. \tag{21}$$

This yields the following RTE for the Fourier component:

$$\mu\frac{\mathrm{d}\mathbf{I}^m(x,\mu)}{\mathrm{d}x}+\mathbf{I}^m(x,\mu)=\frac{\omega}{2}\sum_{l=m}^{LM}\mathbf{P}_l^m(\mu)\mathbf{B}_l\int_{-1}^{1}\mathbf{P}_l^m(\mu')\mathbf{I}^m(x,\mu')\,\mathrm{d}\mu'+\mathbf{Q}^m(x,\mu). \tag{22}$$

Here, the source term is written:

$$\mathbf{Q}^m(x,\mu)=\frac{\omega}{2}\sum_{l=m}^{LM}\mathbf{P}_l^m(\mu)\mathbf{B}_l\mathbf{P}_l^m(-\mu_0)\mathbf{I}_0T_a\mathrm{e}^{-\lambda x}. \tag{23}$$

The phase matrix expansion is expressed through the two matrices:

$$\mathbf{B}_l=\begin{pmatrix}\beta_l & \gamma_l & 0 & 0\\ \gamma_l & \alpha_l & 0 & 0\\ 0 & 0 & \varsigma_l & -\varepsilon_l\\ 0 & 0 & \varepsilon_l & \delta_l\end{pmatrix}, \tag{24}$$

$$\mathbf{P}_l^m(\mu)=\begin{pmatrix}P_l^m(\mu) & 0 & 0 & 0\\ 0 & R_l^m(\mu) & -T_l^m(\mu) & 0\\ 0 & -T_l^m(\mu) & R_l^m(\mu) & 0\\ 0 & 0 & 0 & P_l^m(\mu)\end{pmatrix}. \tag{25}$$

The "Greek matrices" $\mathbf{B}_l$ for $0\leqslant l\leqslant$ LM contain the sets of expansion coefficients that define the scattering law. The $\mathbf{P}_l^m(\mu)$ matrices contain entries of normalized Legendre functions $P_l^m(\mu)$ and functions $R_l^m(\mu)$ and $T_l^m(\mu)$ which are related to $P_{mn}^l(\mu)$ (for details, see for example [19]).

2.3. Boundary conditions

Discrete ordinate RT is pure scattering theory: in a multilayer medium, it is only necessary to specify the layer total optical thickness values Δ_n, the layer total single scatter albedo ω_n, and the layer 4×4 matrices $\mathbf{B}_{nl}$ of expansion coefficients (l being the moment number) for the total scattering. To complete the calculation of the radiation field in a stratified multilayer medium, we have the following boundary conditions:

(I) No diffuse downwelling radiation at TOA. Thus for the first layer we have:

$$\mathbf{I}_n^+(0,\mu,\phi) = 0 \quad (n=1). \tag{26}$$

(II) Continuity of the upwelling and downwelling radiation fields at intermediate boundaries. If N_{TOTAL} is the number of layers in the medium, then:

$$\mathbf{I}_{n-1}^{\pm}(\Delta_{n-1}) = \mathbf{I}_n^{\pm}(0) \quad (n=2,\ldots N_{\mathrm{TOTAL}}). \tag{27}$$

(III) A surface reflection condition relating the upwelling and downwelling radiation fields at the bottom of the atmosphere [53]:

$$\mathbf{I}_n^-(\Delta_n,\mu,\phi) = \mathbf{R}(\mu,\phi;\mu',\phi')\mathbf{I}_n^+(\Delta_n,\mu',\phi') \quad (n=N_{\mathrm{TOTAL}}). \tag{28}$$

Here, reflection matrix $\mathbf{R}$ relates incident and reflected directions.

The convention adopted here is to use a "+" suffix for downwelling solutions, and a "−" suffix for upwelling radiation. Conditions (I) and (II) are obeyed by all Fourier components in the azimuthal series. For condition (III), it is necessary to construct a Fourier decomposition of the BRDF operator $\mathbf{R}$ to separate the azimuth dependence; we return to this issue in Section 5.3. The Lambertian case (isotropic reflectance) only applies for Fourier component $m=0$ and Eq. (28) then becomes [19]:

$$\mathbf{I}_n^-(\Delta_n,\mu) = 2\delta_{m,0}R_0\mathbf{E}_1\left[\mu_0\mathbf{I}_0T_{n-1}\exp(-\lambda_n\Delta_n) + \int_0^1 \mathbf{I}_n^+(\Delta_n,\mu')\mu'\,\mathrm{d}\mu'\right]. \tag{29}$$

Here, R_0 is the Lambertian albedo, $\mathbf{E}_1 = diag\{1,0,0,0\}$, and $T_{n-1}\exp(-\lambda_n\Delta_n)$ is the whole-atmosphere slant path optical depth for the solar beam.

2.4. Jacobian definitions

Atmospheric Jacobians (also known as weighting functions) are *normalized analytic derivatives* of the Stokes vector field with respect to any atmospheric property ξ_{n} defined in layer n:

$$\mathbf{K}_\xi(x,\mu,\phi) = \xi\frac{\partial\mathbf{I}(x,\mu,\phi)}{\partial\xi}. \tag{30}$$

The Fourier series azimuth dependence (Eq. (15)) is also valid:

$$\mathbf{K}_\xi(x,\mu,\phi) = \frac{1}{2}\sum_{l=m}^{LM}(2-\delta_{m,0})\mathbf{C}^m(\phi-\phi_0)\mathbf{K}_\xi^m(x,\mu). \tag{31}$$

We use the linearization notation:

$$\mathscr{L}_p(y_n) = \xi_p\frac{\partial y_n}{\partial\xi_p} \tag{32}$$

to indicate the normalized derivative of y_n in layer n with respect to variable ξ_p in layer p.

As noted in section 2.3, for the radiation field, input optical properties are $\{\Delta_n, \omega_n, \mathbf{B}_{nl}\}$ for each layer n in a multilayer medium. For Jacobians, we require an additional set of *linearized optical property inputs* $\{\mathscr{V}_n, \mathscr{U}_n, \mathscr{Z}_{nl}\}$ defined with respect to variable ξ_n in layer n for which we require weighting functions.

These are:

$$\mathscr{V}_n \equiv \mathscr{L}_n(\Delta_n), \quad \mathscr{U}_n \equiv \mathscr{L}_n(\omega_n), \quad {}_{nl}\mathscr{Z} \equiv \mathscr{L}_n(\mathbf{B}_{nl}). \tag{33}$$

In Section 4.3 we give an example of input sets $\{\Delta_n,\omega_n,\mathbf{B}_{nl}\}$ and their linearizations $\{\mathscr{V}_n,\mathscr{U}_n,\mathscr{Z}_{nl}\}$ for a typical atmospheric scenario with molecular and aerosol scattering. One can also define weighting functions with respect to the basic optical properties: for example, if $\xi_n = \Delta_n$, then $\mathscr{V}_n \equiv \mathscr{L}_n(\Delta_n) = \Delta_n$. It turns out that all weighting functions can be derived from a basic set of Jacobians defined with respect to $\{\Delta_n, \omega_n, \mathbf{B}_{nl}\}$; we return to this point in Section 6.2.

For surface weighting functions, we need to know how the BRDF matrix operator $\mathbf{R}$ in Eq. (28) is parameterized. In VLIDORT, we have adopted a 3-kernel BRDF formulation of surface reflectance similar to the scheme developed in [31] for LIDORT. In Section 4, we confine our attention to the Lambertian case, and discuss the BRDF implementation later in Section 5.3.

2.5. Solution strategy

The solution strategy has two stages. First, for each layer, we establish discrete ordinate solutions to the homogeneous RTE (in the absence of sources) and to the RTE with solar source term (Section 3). Second, we complete the solution by application of boundary conditions and by source function integration of the RTE in order to establish solutions away from discrete ordinate directions (Section 4). In Section 5, we finish the VLIDORT description with a summary of the delta-M approximation, an exact single-scatter treatment, and the use of a 3-kernel BRDF model.

The complete vector RT solution for a plane-parallel slab was developed by Siewert [19], and we follow some elements in this formulation. Our description also adheres closely to the LIDORT treatment, especially concerning this particular integral solution, formulation of the boundary-value problem and linearization methodology.

In the following sections, we suppress the Fourier index m unless noted explicitly, and wavelength dependence is implicit throughout. We sometimes suppress the layer index n in the interests of clarity. For matrix notation, ordinary 4×1 vectors and 4×4 matrices are written in bold typeface, while $4N\times 1$ vectors and $4N\times 4N$ matrices are written in bold typeface with a tilde symbol (N is the number of discrete ordinate directions in the half-space).

3. Discrete ordinate solutions and linearizations

3.1. Homogeneous RTE, eigenproblem reduction

We solve Eq. (22) without the solar source term. For each Fourier term m, the multiple scatter integral over the upper and lower polar direction half-spaces is approximated by a double Gaussian quadrature scheme [54], with stream directions $\{\pm\mu_i\}$ and Gauss–Legendre weights $\{w_i\}$ for i = 1,…N. The resulting vector RTE for Fourier component m is then:

$$\pm\mu_i \frac{\mathrm{d}\mathbf{I}_i^{\pm}(x)}{\mathrm{d}x} \pm \mathbf{I}_i^{\pm}(x) = \frac{\omega_n}{2}\sum_{l=m}^{LM}\mathbf{P}_l^m(\pm\mu_i)\mathbf{B}_l\sum_{j=1}^{N} w_j\left\{\mathbf{I}_j^{+}(x)\mathbf{P}_l^m(\mu_j) + \mathbf{I}_j^{-}(x)\mathbf{P}_l^m(-\mu_j)\right\}. \tag{34}$$

Eq. (34) is a set of $8N$ coupled first-order linear differential equations for $\mathbf{I}_i^{\pm}(x)$. As with the scalar case, these are solved by eigenvalue methods. We follow [19] for the most part. Solutions for these homogeneous equations are found with the *ansatz*:

$$\mathbf{I}_\alpha^{\pm}(x,\pm\mu_i) = \mathbf{W}_\alpha(\pm\mu_i)\exp[-k_\alpha x]. \tag{35}$$

We define the $(4N\times 1)$ vector (superscript "T" denotes matrix transpose):

$$\tilde{\mathbf{W}}_\alpha^{\pm} = \left[\mathbf{W}_\alpha^{\mathrm{T}}(\pm\mu_1), \mathbf{W}_\alpha^{\mathrm{T}}(\pm\mu_2), \ldots, \mathbf{W}_\alpha^{\mathrm{T}}(\pm\mu_N)\right]^{\mathrm{T}}. \tag{36}$$

Eqs. (34) are decoupled using $\tilde{\mathbf{X}}_\alpha = \tilde{\mathbf{W}}_\alpha^+ + \tilde{\mathbf{W}}_\alpha^-$ and $\tilde{\mathbf{Y}}_\alpha = \tilde{\mathbf{W}}_\alpha^+ - \tilde{\mathbf{W}}_\alpha^-$ (sum and difference vectors), and the order of the system can then be reduced from $8N$ to $4N$. This gives an eigenproblem for the collection of separation constants $\{k_\alpha\}$ and associated solution $4N$-vectors $\{\tilde{\mathbf{X}}_\alpha\}$, where $\alpha = 1,\ldots 4N$. The eigenmatrix $\tilde{\mathbf{\Gamma}}$ is constructed from optical property inputs ω and $\mathbf{B}_l$ and products of the matrices $\mathbf{P}_l^m(\mu_j)$. The eigenproblem is [19]:

$$\tilde{\mathbf{X}}_\alpha^\perp \tilde{\mathbf{\Gamma}} = k_\alpha^2 \tilde{\mathbf{X}}_\alpha^\perp, \quad \tilde{\mathbf{\Gamma}} \tilde{\mathbf{X}}_\alpha = k_\alpha^2 \tilde{\mathbf{X}}_\alpha, \tag{37}$$

$$\tilde{\mathbf{\Gamma}} = \tilde{\mathbf{S}}^+ \tilde{\mathbf{S}}^-, \tag{38}$$

$$\tilde{\mathbf{S}}^\pm = \left[\tilde{\mathbf{E}} - \frac{\omega}{2} \sum_{l=m}^{LM} \tilde{\mathbf{\Pi}}(l,m) \mathbf{B}_l \mathbf{A}^\pm \tilde{\mathbf{\Pi}}^{\mathrm{T}}(l,m) \tilde{\mathbf{\Omega}}\right] \tilde{\mathbf{M}}^{-1}, \tag{39}$$

$$\tilde{\mathbf{\Pi}}(l,m) = diag\left[\mathbf{P}_l^m(\mu_1), \mathbf{P}_l^m(\mu_2), ..., \mathbf{P}_l^m(\mu_N)\right]^T, \tag{40}$$

$$\tilde{\mathbf{M}} = diag\left[\mu_1 \mathbf{E}, \mu_2 \mathbf{E}, ..., \mu_N \mathbf{E}\right], \tag{41}$$

$$\tilde{\mathbf{\Omega}} = diag[w_1 \mathbf{E}, w_2 \mathbf{E}, ..., w_N \mathbf{E}], \tag{42}$$

$$\mathbf{A}^\pm = \mathbf{E} \pm (-1)^{l-m} \mathbf{D}. \tag{43}$$

Here, $\mathbf{E}$ is the 4×4 identity matrix, and $\tilde{\mathbf{E}}$ the $4N \times 4N$ identity matrix. The ($\perp$) superscript indicates the conjugate transpose. The link between the eigenvector $\tilde{\mathbf{X}}_\alpha$ and the solution vectors in Eq. (35) is through the auxiliary equations:

$$\tilde{\mathbf{W}}_\alpha^\pm = \frac{1}{2} \tilde{\mathbf{M}}^{-1} \left[\tilde{\mathbf{E}} \pm \frac{1}{k_\alpha} \tilde{\mathbf{S}}^+\right] \tilde{\mathbf{X}}_\alpha. \tag{44}$$

Eigenvalues occur in pairs $\{\pm k_\alpha\}$. As noted by Siewert [19], both complex variable and real-variable eigensolutions may be present. Left and right eigenvectors share the same spectrum of eigenvalues. Solutions may be determined with the complex-variable eigensolver DGEEV from the LAPACK suite [55]. DGEEV returns eigenvalues plus left- and right-eigenvectors with unit modulus.

In the scalar case, the formulation of the eigenproblem is simpler (see [29] for example). The eigenmatrix can be made symmetric and all eigensolutions are real-valued. In this case, the eigensolver module ASYMTX [16] is used. ASYMTX is a modification of the LAPACK routine for real roots; it delivers only the right eigenvectors. For the vector case, there are circumstances (pure Rayleigh scattering for example) where complex eigensolutions are absent, and one may then use the faster ASYMTX routine. We return to this point in Section 6.4.

The complete homogeneous solution in one layer is a linear combination of all positive and negative eigensolutions:

$$\tilde{\mathbf{I}}_+(x) = \tilde{\mathbf{D}}^+ \sum_{\alpha=1}^{4N} \left\{ L_\alpha \tilde{\mathbf{W}}_\alpha^+ \exp[-k_\alpha x] + M_\alpha \tilde{\mathbf{W}}_\alpha^- \exp[-k_\alpha(\Delta - x)] \right\}, \tag{45}$$

$$\tilde{\mathbf{I}}_-(x) = \tilde{\mathbf{D}}^- \sum_{\alpha=1}^{4N} \left\{ L_\alpha \tilde{\mathbf{W}}_\alpha^- \exp[-k_\alpha x] + M_\alpha \tilde{\mathbf{W}}_\alpha^+ \exp[-k_\alpha(\Delta - x)] \right\}. \tag{46}$$

Here, $\tilde{\mathbf{D}}^- = diag\{\mathbf{D}, \mathbf{D}, ..., \mathbf{D}\}$ and $\tilde{\mathbf{D}}^+ = \tilde{\mathbf{E}}$. The use of optical thickness $\Delta - x$ in the second exponential ensures that solutions remain bounded [56]. The quantities $\{L_\alpha, M_\alpha\}$ are the constants of integration, and must be determined by the boundary conditions.

In Eqs. (45) and (46), some eigensolutions will be complex, some real. It is understood that when we use these expressions in the boundary value problem (Section 4.1), we compute the real parts of any contributions to the Stokes vectors resulting from complex eigensolutions. Thus if $\{k_\alpha, \tilde{\mathbf{W}}_\alpha^+\}$ is a complex solution with

(complex) integration constant L_α, we require:

$$\mathrm{Re}[L_\alpha \tilde{\mathbf{W}}_\alpha^- \mathrm{e}^{-k_\alpha x}] = \mathrm{Re}[L_\alpha]\mathrm{Re}[\tilde{\mathbf{W}}_\alpha^- \mathrm{e}^{-k_\alpha x}] - \mathrm{Im}[L_\alpha]\mathrm{Im}[\tilde{\mathbf{W}}_\alpha^- \mathrm{e}^{-k_\alpha x}]. \tag{47}$$

From a bookkeeping standpoint, one must keep count of the number of real and complex solutions, and treat them separately in the numerical implementation. In the interests of clarity, we have not made an explicit separation of complex variables, and it will be clear from the context whether real or complex variables are under consideration.

3.2. Linearization of the eigenproblem

We require derivatives of the above eigenvectors and separation constants with respect to some *atmospheric* variable ξ in layer n. From (38) and (39), the eigenmatrix $\tilde{\mathbf{\Gamma}}$is a linear function of the single scatter albedo ω and the matrix of expansion coefficients $\mathbf{B}_l$, and its (real-variable) linearization $\mathscr{L}(\tilde{\mathbf{\Gamma}})$ is easy to establish from chain-rule differentiation:

$$\mathscr{L}(\tilde{\mathbf{\Gamma}}) = \mathscr{L}(\tilde{\mathbf{S}}^+)\tilde{\mathbf{S}}^- + \tilde{\mathbf{S}}^+\mathscr{L}(\tilde{\mathbf{S}}^-), \tag{48}$$

$$\mathscr{L}\left(\tilde{\mathbf{S}}^\pm\right) = \left[\sum_{l=m}^{LM}\left\{\frac{\mathscr{L}(\omega)}{2}\tilde{\mathbf{\Pi}}(l,m)\mathbf{B}_l + \frac{\omega}{2}\tilde{\mathbf{\Pi}}(l,m)\mathscr{L}(\mathbf{B}_l)\right\}\mathbf{A}^\pm\tilde{\mathbf{\Pi}}^{\mathrm{T}}(l,m)\tilde{\mathbf{\Omega}}\right]\tilde{\mathbf{M}}^{-1}. \tag{49}$$

In Eq. (49), $\mathscr{L}(\omega) = \mathscr{U}$ and $\mathscr{L}(\mathbf{B}_l) = \mathscr{Z}_l$ are the linearized optical property inputs (Eq. (33)). Next, we differentiate both the left and right eigensystems (37) to find:

$$\mathscr{L}\left(\tilde{\mathbf{X}}_\alpha^\perp\right)\tilde{\mathbf{\Gamma}} + \tilde{\mathbf{X}}_\alpha^\perp\mathscr{L}\left(\tilde{\mathbf{\Gamma}}\right) = 2k_\alpha\mathscr{L}(k_a)\tilde{\mathbf{X}}_\alpha^\perp + k_\alpha^2\mathscr{L}\left(\tilde{\mathbf{X}}_\alpha^\perp\right), \tag{50}$$

$$\tilde{\mathbf{\Gamma}}\mathscr{L}(\tilde{\mathbf{X}}_\alpha) + \mathscr{L}(\tilde{\mathbf{\Gamma}})\tilde{\mathbf{X}}_\alpha = 2k_\alpha\mathscr{L}(k_\alpha)\tilde{\mathbf{X}}_\alpha + k_\alpha^2\mathscr{L}(\tilde{\mathbf{X}}_\alpha). \tag{51}$$

We form a dot product by pre-multiplying (51) with the transpose vector $\tilde{\mathbf{X}}_\alpha^\perp$, rearranging to get:

$$2k_\alpha\mathscr{L}(k_\alpha)\langle\tilde{\mathbf{X}}_\alpha^\perp, \tilde{\mathbf{X}}_\alpha\rangle - \langle\tilde{\mathbf{X}}_\alpha^\perp, \mathscr{L}(\tilde{\mathbf{\Gamma}})\tilde{\mathbf{X}}_\alpha\rangle = k_\alpha^2\langle\tilde{\mathbf{X}}_\alpha^\perp, \mathscr{L}(\tilde{\mathbf{X}}_\alpha)\rangle - \langle\tilde{\mathbf{X}}_\alpha^\perp, \tilde{\mathbf{\Gamma}}\mathscr{L}(\tilde{\mathbf{X}}_\alpha)\rangle. \tag{52}$$

From the definitions in Eq. (37), we have:

$$\langle\tilde{\mathbf{X}}_\alpha^\perp, \tilde{\mathbf{\Gamma}}\mathscr{L}(\tilde{\mathbf{X}}_\alpha)\rangle = \langle\tilde{\mathbf{X}}_\alpha^\perp\tilde{\mathbf{\Gamma}}, \mathscr{L}(\tilde{\mathbf{X}}_\alpha)\rangle = k_\alpha^2\langle\tilde{\mathbf{X}}_\alpha^\perp, \mathscr{L}(\tilde{\mathbf{X}}_\alpha)\rangle \tag{53}$$

and hence the right-hand side of (52) is identically zero. We thus have:

$$\mathscr{L}(k_\alpha) = \frac{\langle\tilde{\mathbf{X}}_\alpha^\perp, \mathscr{L}(\tilde{\mathbf{\Gamma}})\tilde{\mathbf{X}}_\alpha\rangle}{2k_\alpha\langle\tilde{\mathbf{X}}_\alpha^\perp, \tilde{\mathbf{X}}_\alpha\rangle}. \tag{54}$$

Next, we substitute Eq. (54) in (52) to obtain the following $4N \times 4N$ linear algebra problem for each eigensolution linearization:

$$\tilde{\mathbf{H}}_\alpha\mathscr{L}\left(\tilde{\mathbf{X}}_\alpha\right) = \tilde{\mathbf{C}}_\alpha, \tag{55}$$

$$\tilde{\mathbf{H}}_\alpha = \tilde{\mathbf{\Gamma}} - k_\alpha^2\tilde{\mathbf{E}}, \tag{56}$$

$$\tilde{\mathbf{C}}_\alpha = 2k_\alpha\mathscr{L}(k_\alpha)\tilde{\mathbf{X}}_\alpha - \mathscr{L}(\tilde{\mathbf{\Gamma}})\tilde{\mathbf{X}}_\alpha. \tag{57}$$

Implementation of Eq. (55) "as is" is not possible due to the degeneracy of the eigenproblem, and we need additional constraints to find the unique solution for $\mathscr{L}(\tilde{\mathbf{X}}_\alpha)$. The treatment for real and complex solutions is different.

Real solutions: The unit-modulus eigenvector normalization can be expressed as $\langle\tilde{\mathbf{X}}_\alpha, \tilde{\mathbf{X}}_\alpha\rangle = 1$ in dot-product notation. Linearizing, this yields one equation:

$$\mathscr{L}(\tilde{\mathbf{X}}_\alpha)\tilde{\mathbf{X}}_\alpha + \tilde{\mathbf{X}}_\alpha\mathscr{L}(\tilde{\mathbf{X}}_\alpha) = 0. \tag{58}$$

The solution procedure uses $4N-1$ equations from (55), along with Eq. (58) to form a slightly modified linear system of rank $4N$. This system is then solved by standard means using the DGETRF and DGETRS LU-decomposition routines from the LAPACK suite.

This procedure was not used in the scalar LIDORT code [28–29]. This is because ASYMTX has no adjoint solution, so there is no determination of $\mathscr{L}(k_\alpha)$ as in Eq. (54). Instead, LIDORT uses the complete set (55) *in addition* to constraint (58) to form a system of rank $N+1$ for the unknowns $\mathscr{L}(k_\alpha)$ and $\mathscr{L}(\tilde{\mathbf{X}}_\alpha)$.

Complex solutions: In this case, Eq. (55) is a complex-variable system for both the real and imaginary parts of the linearized eigenvectors. There are $8N$ equations in all, but now we require two constraint conditions to remove the eigenproblem arbitrariness. The first is Eq. (58). The second condition is imposed by the following DGEEV normalization: for that element of an eigenvector with the largest real value, the corresponding imaginary part is always set to zero. Thus for an eigenvector $\tilde{\mathbf{X}}$, if element $\mathrm{Re}[X_J] = \max\{\mathrm{Re}[X_j]\}$ for $j = 1,\ldots 4N$, then $\mathrm{Im}[X_J] = 0$. In this case, it is also true that $L(\mathrm{Im}[X_J]) = 0$. This is the second condition.

The solution procedure is then (1) in Eq. (55) to strike out the row and column J in matrix $\tilde{\mathbf{H}}_\alpha$ for which the quantity $\mathrm{Im}[X_J]$ is zero, and strike out the corresponding row in the right-hand vector $\tilde{\mathbf{C}}_\alpha$; and (2) in the resulting $8N1$ system, replace one of the rows with the normalization constraint Eq. (58). $\mathscr{L}(\tilde{\mathbf{X}}_\alpha)$ is then the solution of the resulting linear system.

We have gone into detail here, as the above procedure for eigensolution differentiation is the most crucial step in the linearization process, and there are several points of departure from the equivalent procedure in the scalar case. Having derived the linearizations $\mathscr{L}(k_\alpha)$ and $\mathscr{L}(\tilde{\mathbf{X}}_\alpha)$, we complete this section by differentiating the auxiliary result in Eq. (44) to establish $\mathscr{L}(\tilde{\mathbf{W}}_\alpha^{\pm})$:

$$\mathscr{L}(\tilde{\mathbf{W}}_\alpha^{\pm}) = \frac{1}{2}\tilde{\mathbf{M}}^{-1}\left[\mp\frac{\mathscr{L}(k_\alpha)}{k_\alpha^2}\tilde{\mathbf{S}}^{+} \pm \frac{1}{k_\alpha}\mathscr{L}(\tilde{\mathbf{S}}^{+})\right]\tilde{\mathbf{X}}_\alpha + \frac{1}{2}\tilde{\mathbf{M}}^{-1}\left[\tilde{\mathbf{E}} \pm \frac{1}{k_\alpha}\tilde{\mathbf{S}}^{+}\right]\mathscr{L}(\tilde{\mathbf{X}}_\alpha). \tag{59}$$

Finally, we have linearizations of the transmittance derivatives in Eqs. (45) and (46):

$$\mathscr{L}(\exp[-k_\alpha x]) = -x\left\{\mathscr{L}(k_\alpha) + k_\alpha\mathscr{L}(x)\right\}\exp[-k_\alpha x]. \tag{60}$$

Here, x and Δ_n are proportional for an optically uniform layer, so that

$$\mathscr{L}_\xi(x) = \frac{x}{\Delta_n}\mathscr{L}_\xi(\Delta_n) = \frac{x}{\Delta_n}\mathscr{V}_\xi. \tag{61}$$

3.3. Particular integrals of the vector RTE

3.3.1. Solving the RTE by substitution

In the treatment of the particular integral solutions of the vector RTE, we use a more traditional substitution method rather than the Green's function formalism of Siewert [19]. This is mainly for reasons of clarity and ease of exposition. Referring to Eq. (23), inhomogeneous source terms in the discrete ordinate directions are:

$$\mathbf{Q}_n^m(x,\pm\mu_i) = \frac{\omega}{2}\sum_{l=m}^{L}\mathbf{P}_l^m(\pm\mu_i)\mathbf{B}_{nl}\mathbf{P}_l^m(-\mu_0)\mathbf{I}_0 T_{n-1}\exp(-\lambda_n x). \tag{62}$$

Here T_{n-1} is the solar beam transmittance to the top of layer n, and in the pseudo-spherical approximation, λ_n is the average secant (Appendix A). Particular solutions may be found by substitution:

$$\mathbf{I}^{\pm}(x,\pm\mu_i) = \mathbf{Z}_n(\pm\mu_i)T_{n-1}\exp[-\lambda_n x] \tag{63}$$

and by analogy with the homogeneous case, we define the $4N\times 1$ vectors:

$$\tilde{\mathbf{Z}}_n^{\pm} = \left[\mathbf{Z}_n^{\mathrm{T}}(\pm\mu_1), \mathbf{Z}_n^{\mathrm{T}}(\pm\mu_2), \ldots., \mathbf{Z}_n^{\mathrm{T}}(\pm\mu_N)\right]^{\mathrm{T}}. \tag{64}$$

We decouple the resulting equations by using sum and difference vectors $\tilde{\mathbf{G}}_n^{\pm} = \tilde{\mathbf{Z}}_n^{+} \pm \tilde{\mathbf{Z}}_n^{-}$, and reduce the order from $8N$ to $4N$ (see [30] for the scalar case). We obtain the following $4N\times 4N$ linear-algebra problem:

$$\tilde{\mathbf{A}}_n^{(2)}\tilde{\mathbf{G}}_n^{+} = \tilde{\mathbf{C}}_n^{(2)}, \tag{65}$$

$$\tilde{\mathbf{A}}_n^{(2)} = \lambda_n^2 \tilde{\mathbf{E}} - \tilde{\mathbf{\Gamma}}_n, \tag{66}$$

$$\tilde{\mathbf{C}}_n^{(2)} = \left[\tilde{\mathbf{S}}_n^- \tilde{\mathbf{Q}}_n^+ + \lambda_n \tilde{\mathbf{Q}}_n^-\right] \tilde{\mathbf{M}}^{-1}, \tag{67}$$

$$\tilde{\mathbf{Q}}_n^{\pm} = \omega \sum_{l=m}^{LM} \tilde{\mathbf{\Pi}}_0(l,m) \mathbf{B}_l \mathbf{A}^{\pm} \tilde{\mathbf{\Pi}}^{\mathrm{T}}(l,m) \tilde{\mathbf{M}}^{-1}, \tag{68}$$

$$\tilde{\mathbf{\Pi}}_0(l,m) = \left[\mathbf{P}_l^m(-\mu_0), \mathbf{P}_l^m(-\mu_0), \ldots, \mathbf{P}_l^m(-\mu_0)\right]^{\mathrm{T}}. \tag{69}$$

This system has some similarities to the eigensolution linearization in Eqs. (55)–(58). It is also solved using the LU-decomposition modules DGETRF and DGETRS from LAPACK; the formal solution is $\tilde{\mathbf{G}}_n^+ = \left[\tilde{\mathbf{A}}_n^{(2)}\right]^{-1} \tilde{\mathbf{C}}_n^{(2)}$. The particular integral is completed through the auxiliary equations:

$$\tilde{\mathbf{Z}}_n^{\pm} = \frac{1}{2} \tilde{\mathbf{M}}^{-1} \left[\tilde{\mathbf{E}} \pm \frac{1}{\lambda_n} \tilde{\mathbf{S}}_n^+\right] \tilde{\mathbf{G}}_n^+. \tag{70}$$

We note that the particular solution consists only of real variables.

3.3.2. Linearizing the particular solution

For the linearization, the most important point is the presence of cross-derivatives: the particular solution is differentiable with respect to atmospheric variables ξ_p in all layers $p \geqslant n$. The solar beam has passed through layer $p \geqslant n$ before scattering, so transmittance factor T_{n-1} depends on variables in layers $p > n$ and the average secant λ_n (in the pseudo-spherical approximation) on variables ξ_p for $p \geqslant n$ In addition, the solution vectors $\tilde{\mathbf{Z}}_n^{\pm}$ depend on λ_n, so *their* linearizations contain cross-derivatives.

Linearization of the pseudo-spherical approximation is treated in Appendix A, and this fixes the quantities $\mathscr{L}_p(T_{n-1})$ and $\mathscr{L}_p(\lambda_n)$ $\forall p \geqslant n$. For the plane-parallel case, $\mathscr{L}_p(\lambda_n) \equiv 0$ since $\lambda_n = -1/\mu_0$ (constant). In addition, the eigenmatrix $\tilde{\mathbf{\Gamma}}_n$ is constructed from optical properties only defined in layer n, so that $\mathscr{L}_p(\tilde{\mathbf{\Gamma}}_n) = 0$ $\forall$ $p \neq n$. Differentiation of Eqs. (65)–(69) yields a related linear problem:

$$\tilde{\mathbf{A}}_n^{(2)} \mathscr{L}_p(\tilde{\mathbf{G}}_n^+) \equiv \tilde{\mathbf{C}}_{np}^{(3)} = \mathscr{L}_p(\tilde{\mathbf{C}}_n^{(2)}) - \mathscr{L}_p(\tilde{\mathbf{A}}_n^{(2)}) \tilde{\mathbf{G}}_n^+, \tag{71}$$

$$\mathscr{L}_p(\tilde{\mathbf{A}}_n^{(2)}) = -\delta_{pn} \mathscr{L}_p(\tilde{\mathbf{\Gamma}}_n) + 2\lambda_n \mathscr{L}_p(\lambda_n) \tilde{\mathbf{E}}, \tag{72}$$

$$\mathscr{L}_p(\tilde{\mathbf{C}}_n^{(2)}) = \delta_{np} \left[\mathscr{L}_p(\tilde{\mathbf{S}}_n^-) \tilde{\mathbf{Q}}_n^+ + \tilde{\mathbf{S}}_n^- \mathscr{L}_n(\tilde{\mathbf{Q}}_n^+) + \frac{1}{\lambda_n} \mathscr{L}_n(\tilde{\mathbf{Q}}_n^-)\right] - \frac{\mathscr{L}_p(\lambda_n)}{\lambda_n^2} \tilde{\mathbf{Q}}_n^-, \tag{73}$$

$$\mathscr{L}_n(\tilde{\mathbf{Q}}_n^{\pm}) = \sum_{l=m}^{LM} \left[\mathscr{U}_n \tilde{\mathbf{\Pi}}_0(l,m) \mathbf{B}_l + \omega_n \tilde{\mathbf{\Pi}}_0(l,m) Z_{nl}\right] \mathbf{A}^{\pm} \tilde{\mathbf{\Pi}}^{\mathrm{T}}(l,m) \tilde{\mathbf{M}}^{-1}. \tag{74}$$

In Eq. (73), the quantity $\mathscr{L}_n(\tilde{\mathbf{S}}_n^-)$ comes from (49). Eq. (71) has the same matrix $\tilde{\mathbf{A}}_n^{(2)}$ as in Eq. (65), but with a different source vector on the right-hand side. The solution is then found by back-substitution, given that the inverse of the matrix $\tilde{\mathbf{A}}_n^{(2)}$ has already been established for the original solution $\tilde{\mathbf{G}}_n^+$. Thus $\mathscr{L}_p(\tilde{\mathbf{G}}_n^+) = \left[\tilde{\mathbf{A}}_n^{(2)}\right]^{-1} \tilde{\mathbf{C}}_{np}^{(3)}$. Linearization of the particular integral is then completed through differentiation of the auxiliary equations (70):

$$\mathscr{L}_p(\tilde{\mathbf{Z}}_n^{\pm}) = \frac{1}{2} \tilde{\mathbf{M}}^{-1} \left[\tilde{\mathbf{E}} \pm \frac{1}{\lambda_n} \tilde{\mathbf{S}}_n^+\right] \mathscr{L}_p(\tilde{\mathbf{G}}_n^+) \mp \frac{1}{2\lambda_n^2} \tilde{\mathbf{M}}^{-1} \left[\lambda_n \delta_{pn} \mathscr{L}_p(\tilde{\mathbf{S}}_n^+) - \mathscr{L}_p(\lambda_n) \tilde{\mathbf{S}}_n^+)\right] \tilde{\mathbf{G}}_n^+. \tag{75}$$

This completes the RTE solution determination and the corresponding linearizations with respect to atmospheric variables.

4. The post-processed solution

4.1. Boundary value problem (BVP) and linearization

From Section 3, the complete Stokes vector discrete ordinate solutions in layer n may be written:

$$\tilde{\mathbf{I}}_n^{\pm}(x) = \tilde{\mathbf{D}}^{\pm} \sum_{\alpha=1}^{4N} \left[L_{n\alpha} \tilde{\mathbf{W}}_{n\alpha}^{\pm} \mathrm{e}^{-k_{n\alpha}x} + M_{n\alpha} \tilde{\mathbf{W}}_{n\alpha}^{\mp} \mathrm{e}^{-k_{n\alpha}(\Delta_n - x)} \right] + \tilde{\mathbf{Z}}_n^{\pm} T_{n-1} \mathrm{e}^{-\lambda_n x}. \tag{76}$$

Quantities $L_{n\alpha}$ and $M_{n\alpha}$ are *constants of integration* for the homogeneous solutions, and they are determined by the imposition of three boundary conditions as noted in Section 2.3. For boundary condition (I), we have $\tilde{\mathbf{I}}_n^{+}(0) = 0$ for $n = 1$, which yields ($T_0 = 1$):

$$\tilde{\mathbf{D}}^{+} \sum_{\alpha=1}^{4N} \left[L_{n\alpha} \tilde{\mathbf{W}}_{n\alpha}^{+} + M_{n\alpha} \tilde{\mathbf{W}}_{n\alpha}^{-} \mathrm{K}_{n\alpha} \right] = -\tilde{\mathbf{Z}}_n^{+}. \tag{77}$$

For boundary condition (II), the continuity at layer boundaries, we have:

$$\begin{aligned} &\tilde{\mathbf{D}}^{\pm} \sum_{\alpha=1}^{4N} \left[\left\{ L_{n\alpha} \tilde{\mathbf{W}}_{n\alpha}^{\pm} \mathrm{K}_{n\alpha} + M_{n\alpha} \tilde{\mathbf{W}}_{n\alpha}^{\mp} \right\} - \left\{ L_{p\alpha} \tilde{\mathbf{W}}_{p\alpha}^{\pm} + M_{p\alpha} \tilde{\mathbf{W}}_{p\alpha}^{\mp} \mathrm{K}_{p\alpha} \right\} \right] \\ &= -\tilde{\mathbf{Z}}_n^{\pm} T_{n-1} \Lambda_n + \tilde{\mathbf{Z}}_p^{\pm} T_{p-1}. \end{aligned} \tag{78}$$

In Eq. (78), $p = n+1$. For surface condition (III), staying for convenience with the Lambertian condition in Eq. (29), we find (for layer $n = N_{\mathrm{TOTAL}}$):

$$\tilde{\mathbf{D}}^{-} \sum_{\alpha=1}^{4N} \left[L_{n\alpha} \tilde{\mathbf{V}}_{\alpha}^{-} \mathrm{K}_{n\alpha} + M_{n\alpha} \tilde{\mathbf{V}}_{\alpha}^{+} \right] = T_{n-1} \Lambda_n \left[-\tilde{\mathbf{U}}^{-} + 2R_0 \mu_0 \tilde{\mathbf{E}}_1 I_0 \right]. \tag{79}$$

Here we have defined the following auxiliary quantities:

$$\tilde{\mathbf{V}}_{\alpha}^{\pm} = \tilde{\mathbf{W}}_{n\alpha}^{\pm} - 2R_0 \tilde{\mathbf{E}}_1^{\mathrm{T}} \tilde{\mathbf{M}} \tilde{\mathbf{\Omega}} \tilde{\mathbf{W}}_{n\alpha}^{\pm} \tilde{\mathbf{E}}_1, \quad (n = N_{\mathrm{TOTAL}}), \tag{80}$$

$$\tilde{\mathbf{U}}^{-} = \tilde{\mathbf{Z}}_n^{-} - 2R_0 \tilde{\mathbf{E}}_1^{\mathrm{T}} \tilde{\mathbf{M}} \tilde{\mathbf{\Omega}} \tilde{\mathbf{Z}}_n^{\pm} \tilde{\mathbf{E}}_1, \quad (n = N_{\mathrm{TOTAL}}), \tag{81}$$

$$\tilde{\mathbf{E}}_1 = diag\{\mathbf{E}_1, \mathbf{E}_1, \ldots \mathbf{E}_1\}. \tag{82}$$

$$\mathrm{K}_{n\alpha} = \mathrm{e}^{-k_{n\alpha}\Delta_n}, \quad \Lambda_n = \mathrm{e}^{-\lambda_n \Delta_n}, \quad (n = 1, \ldots, N_{\mathrm{TOTAL}}). \tag{83}$$

Application of Eqs. (77)–(79) yields a large, sparse banded linear system with rank $8N \times N_{\mathrm{TOTAL}}$. This system consists only of real variables, and may be written in the symbolic form:

$$\mathbf{\Phi} * \mathbf{\Xi} = \mathbf{\Psi}. \tag{84}$$

Here $\mathbf{\Psi}$ is constructed from the right hand-side variables in Eqs. (77)–(79) and $\mathbf{\Phi}$ is constructed from suitable combinations of $\tilde{\mathbf{V}}_{\alpha}^{\pm}, \tilde{\mathbf{W}}_{n\alpha}^{\pm}$ and $\mathrm{K}_{n\alpha}$. For a visualization of the BVP in the scalar case, see [28]. The vector $\mathbf{\Xi}$ of integration constants is made up of the unknowns $\{L_{n\alpha}, M_{n\alpha}\}$ and will be partitioned into contributions from real and complex parts. A schematic of this partitioning is shown in Fig. 1.

The solution proceeds first by the application of a compression algorithm to reduce the order and eliminate redundant zero entries. LU-decomposition is then applied using the banded-matrix LAPACK routine DGBTRF to find the inverse $\mathbf{\Phi}^{-1}$, and the final answer $\mathbf{\Xi} = \mathbf{\Phi}^{-1} * \mathbf{\Psi}$ is then obtained by back-substitution (using DGBTRS). For the slab problem, boundary condition (II) is absent; the associated linear problem is then solved using the DGETRF/DGETRS combination.

Linearizing Eq. (84) with respect to a variable ξ_p in layer p, we obtain:

$$\mathbf{\Phi} * \mathscr{L}_p(\mathbf{\Xi}) = \mathbf{\Psi}'_p \equiv \mathscr{L}_p(\mathbf{\Psi}) - \mathscr{L}_p(\mathbf{\Phi}) * \mathbf{\Xi}. \tag{85}$$

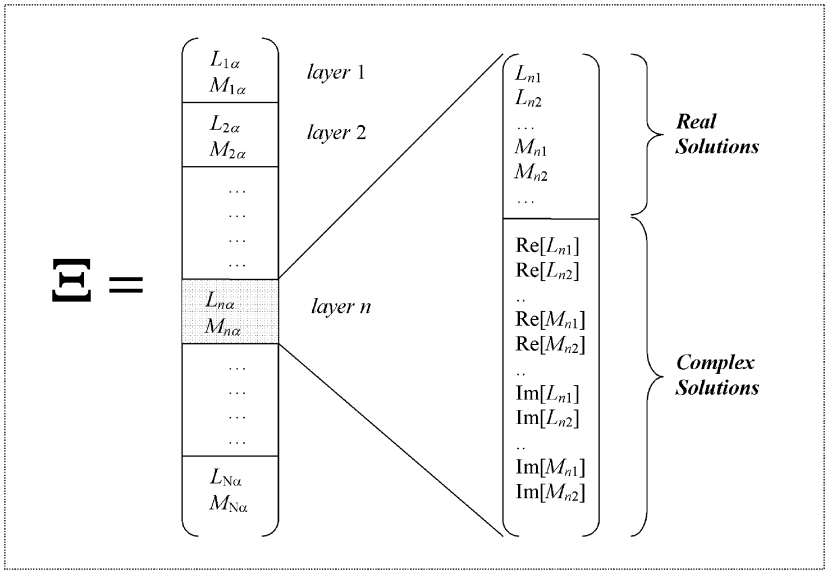

Fig. 1. Schematic breakdown of the vector of integration constants to be determined as the solution to the boundary value problem in a multilayer atmosphere.

We notice that this is the same linear-algebra problem, but now with a different source vector $\boldsymbol{\Psi}'_p$ on the right-hand side. Since we already have the inverse $\boldsymbol{\Phi}^{-1}$ from the solution to the original BVP, back-substitution gives the linearization $\mathscr{L}_p(\boldsymbol{\Xi}) = \boldsymbol{\Phi}^{-1} * \boldsymbol{\Psi}'_p$ of the boundary value constants. Although this linearization is straightforward in concept, there are many algebraic details arising with chain rule differentiation required to establish $\mathscr{L}_p(\boldsymbol{\Psi})$ and $\mathscr{L}_p(\boldsymbol{\Phi})$ in Eq. (85).

4.2. Source function integration

The source function integration technique is used to determine solutions at off-quadrature polar directions μ and at arbitrary optical thickness values in the multilayer medium. The technique dates back to the work of Chandrasekhar [1], and has been demonstrated to be superior to numerical interpolation. We substitute layer discrete ordinate solutions (76) into the multiple scattering integral in Eq. (22), then integrate over optical thickness. The methodology follows closely that used for the scalar LIDORT code [28–30], so long as we remember with the Stokes-vector formulation to use the real part of any quantity derived from combinations of complex-variable entities. Here, we note down the principal results for the upwelling field.

The solution in layer n at direction μ for optical thickness x (as measured from the top of the layer) is given by:

$$\mathbf{I}_n^-(x,\mu) = \mathbf{I}_n^-(\Delta,\mu)\mathrm{e}^{-(\Delta-x)/\mu} + \mathbf{H}_n^-(x,\mu) + \big(\mathbf{Z}_n^-(\mu) + \mathbf{Q}_n^-(\mu)\big)\mathscr{E}_n^-(x,\mu). \tag{86}$$

The first term is the upward transmission of the lower-boundary Stokes vector field through a partial layer of optical thickness $\Delta - x$. The other three contributions together constitute the *partial layer source term* due to scattered light contributions. The first of these three is due to the homogeneous solutions and has the form:

$$\mathbf{H}_n^-(x,\mu) = \sum_{\alpha=1}^{4N}\big[L_{n\alpha}\mathbf{X}_{n\alpha}^+(\mu)\mathscr{H}_{n\alpha}^{-+}(x,\mu) + M_{n\alpha}\mathbf{X}_{n\alpha}^-(\mu)\mathscr{H}_{n\alpha}^{--}(x,\mu)\big], \tag{87}$$

where we have defined the following auxiliary quantities:

$$\mathbf{X}_{n\alpha}^{\pm}(\mu) = \frac{\omega}{2}\sum_{l=m}^{LM}\mathbf{P}_l^m(\mu)\mathbf{B}_{nl}\sum_{j=1}^{N} w_j\big\{\mathbf{P}_l^m(\mu_j)\mathbf{X}_{n\alpha}^{\pm}(\mu_i) + \mathbf{P}_l^m(-\mu_j)\mathbf{X}_{n\alpha}^{\pm}(-\mu_i)\big\}, \tag{88}$$

$$\mathscr{H}^{-+}_{n\alpha}(x,\mu) = \frac{\mathrm{e}^{-xk_{n\alpha}} - \mathrm{e}^{-\Delta_n k_{n\alpha}}\mathrm{e}^{-(\Delta_n - x)/\mu}}{1+\mu k_{n\alpha}}. \tag{89}$$

$$\mathscr{H}^{--}_{n\alpha}(x,\mu) = \frac{\mathrm{e}^{-(\Delta_n - x)k_{n\alpha}} - \mathrm{e}^{-(\Delta_n - x)/\mu}}{1-\mu k_{n\alpha}}. \tag{90}$$

Here, $\mathbf{X}^{\pm}_{n\alpha}(\mu)$ are homogeneous solutions defined at stream cosine μ, and $\mathscr{H}^{-\pm}_{n\alpha}(x,\mu)$ are the *homogeneous solution multipliers* for the upwelling field. These multipliers arise from the layer optical thickness integration. In (87), we consider only the real value of the resulting expressions.

The other two layer source term contributions in Eq. (86) come from the diffuse and direct solar source scattering, respectively. In this case, all variables are real numbers, and the relevant quantities are:

$$\mathbf{Z}^{-}_{n}(\mu) = \frac{\omega}{2}\sum_{l=m}^{LM}\mathbf{P}^{m}_{l}(\mu)\mathbf{B}_{nl}\sum_{j=1}^{N} w_j\left\{\mathbf{P}^{m}_{l}(\mu_j)\mathbf{Z}^{-}_{n}(\mu_j) + \mathbf{P}^{m}_{l}(-\mu_j)\mathbf{Z}^{-}_{n}(-\mu_j)\right\}, \tag{91}$$

$$\mathbf{Q}^{-}_{n}(\mu) = \frac{\omega(2-\delta_{m0})}{2}\sum_{l=m}^{LM}\mathbf{P}^{m}_{l}(\mu_i)\mathbf{B}_{nl}\mathbf{P}^{m}_{l}(-\mu_0)\mathbf{I}_0, \tag{92}$$

$$\mathscr{E}^{-}_{n}(x,\mu) = T_{n-1}\frac{\mathrm{e}^{-x\lambda_n} - \mathrm{e}^{-\Delta_n\lambda_n}\mathrm{e}^{-(\Delta_n - x)/\mu}}{1+\mu\lambda_n}. \tag{93}$$

These expressions have counterparts in the scalar code (see for example [29]). Similar expressions can be written for post-processing of downwelling solutions. All source term quantities can be expressed in terms of the basic optical property inputs to VLIDORT $\{\Delta_n, \omega_n, \mathbf{B}_{nl}\}$, the pseudo-spherical beam transmittance quantities $\{T_n, \lambda_n\}$, the homogeneous solutions $\{k_{n\alpha}, \tilde{\mathbf{X}}^{\pm}_{n\alpha}\}$, the particular solutions $\tilde{\mathbf{Z}}^{\pm}_{n}$, and the BVP integration constants $\{L_{n\alpha}, M_{n\alpha}\}$.

Linearizations: Derivatives of all these expressions may be determined by differentiation with respect to variable ξ_n in layer n. The end-points of the chain rule differentiation are the linearized optical property inputs $\{\mathscr{V}_n, \mathscr{U}_n, \mathscr{Z}_{nl}\}$ from Eq. (33). For linearization of the *homogeneous* post-processing source term in layer n, there is no dependency on any quantities outside of layer n; in other words, $\mathscr{L}_p[\mathbf{H}^{-}_{n}(x,\mu)] \equiv 0$ for $p \neq n$. The *particular* solution post-processing source terms in layer n depend on optical thickness values in all layers above and equal to n through the presence of the average secant and the solar beam transmittances, so there will be cross-layer derivatives. However, the chain-rule differentiation method is the same, and requires a careful exercise in algebraic manipulation.

Multiplier expressions (89), (90) and (93) have appeared a number of times in the literature. The linearizations were discussed in [29,30], and we need only make two remarks here. Firstly, the real and complex homogeneous solution multipliers are treated separately, with the real part of the complex variable result to be used in the final reckoning. Second, the solar source term multipliers (for example in Eq. (93)) are *the* same as those in the scalar model.

5. Additional VLIDORT implementations

5.1. The delta-M approximation

In the scalar model, sharply peaked phase functions are approximated as a combination of a delta-function and a smoother residual phase function. This is the delta-M approximation [57], which is widely used in discrete ordinate and other RT models. The delta-M scaled optical property inputs (optical thickness, single scatter albedo, phase function Legendre expansion coefficients) are:

$$\bar{\tau} = \tau(1-\omega f), \quad \bar{\omega} = \omega\frac{(1-f)}{(1-\omega f)}, \quad \bar{\beta}_l = \frac{\beta_l - f(2l+1)}{(1-f)}. \tag{94}$$

The delta-M truncation factor is

$$f = \frac{\beta_{2N}}{(2N+1)}. \tag{95}$$

In VLIDORT, Legendre coefficients β_l appear as the (1,1) entry in matrix $\mathbf{B}_l$. In line with the scalar definition in terms of the phase function, we take in VLIDORT the truncation factor f as defined Eq. (95), and adopt the following scaling for the six entries in $\mathbf{B}_l$. Four coefficients (α_l, β_l, ζ_l and δ_l) will scale as β_l in Eq. (94), while the other two coefficients γ_l and ε_l scale as $\tilde{\gamma}_l = \gamma_l/(1-f)$. This specification can also be found in [58] where a more detailed justification is presented. Scaling for the optical thickness and single scatter albedo in Eq. (94) is not changed in the vector model. Linearizations of Eqs. (94) and (95) are straightforward, and these are discussed in [29] for the scalar model.

5.2. Exact single scatter solutions

In VLIDORT, we include an exact single-scatter computation based on the Nakajima–Tanaka (N–T) procedure [59]. The internal single scatter computation in VLIDORT will use a truncated subset of the complete scatter-matrix information, the number of usable Legendre coefficient matrices $\mathbf{B}_l$ being limited to $2N-1$ for N discrete ordinate streams. A more accurate computation can be made if the post-processing calculation of the single scatter contribution (the term $\mathbf{Q}_n^-(\mu)\mathscr{E}_n^-(x,\mu)$ in Eq. (86) for example) is suppressed in favor of an accurate single scatter computation, which uses the complete phase matrix. The N-T correction procedure appears in the DISORT [60] and scalar LIDORT codes [29–32], and a related computation has been implemented for the doubling-adding method [14].

The (upwelling) post-processed solution in stream direction μ is now written (c.f. Eq. (86)):

$$\mathbf{I}_n^-(x,\mu) = \mathbf{I}_n^-(\Delta,\mu)\mathrm{e}^{-(\Delta-x)/\mu} + \mathbf{H}_n^-(x,\mu) + \left(\mathbf{Z}_n^-(\mu) + \mathbf{Q}_{n,\mathrm{exact}}^-(\mu)\right)\mathscr{E}_n^-(x,\mu) \tag{96}$$

$$\mathbf{Q}_{n,\mathrm{exact}}^-(\mu) = \frac{\omega_n}{4\pi(1-\omega_n f_n)}\mathbf{\Pi}_n(\mu,\mu_0,\phi-\phi_0)\mathbf{I}_0. \tag{97}$$

Note the presence of denominator $(1-\omega_n f_n)$ when the delta-M approximation is in force [59]. From section 2.1, $\mathbf{\Pi}_n$ is obtained from the scattering matrix $\mathbf{F}_n(\Theta)$ through application of rotation matrices. There is no truncation: $\mathbf{\Pi}_n$ can be constructed to any degree of accuracy using all available unscaled Greek matrices $\mathbf{B}_{nl}$.

Linearization: Chain-rule differentiation of Eq. (97) yields the linearization of the exact single scatter correction term. Linearization of the multiplier $\mathscr{E}_n^-(x,\mu)$ has already been established. Since the elements of $\mathbf{\Pi}_n$ consist of linear combinations of $\mathbf{B}_{\mathrm{nl}}$, the linearization $\mathscr{L}_n(\mathbf{\Pi}_n)$is straightforward to write down in terms of the inputs $\mathscr{L}_n(\mathbf{B}_{nl})$.

Curved line-of-sight paths: For nadir-geometry satellite instruments with wide-angle off-nadir viewing, one must consider the Earth's curvature along the line of sight from the ground to the satellite. This applies to instruments such as OMI on the Aura platform (swath 2600 km, scan angle 114° at the satellite) [61] and GOME-2 (swath 1920 km) [44]. Failure to account for this effect can lead to errors of 5–10% in the satellite radiance for TOA viewing zenith angles in the range 55–70° [31,57,58]. For LIDORT, a simple correction for this effect was introduced for satellite geometries in [31] and this applies equally to VLIDORT. Correction involves an exact single scatter calculation along the line of sight from ground to TOA: in this case, Eq. (97) is still valid, but now the geometry is changing from layer to layer. We give a brief summary of this implementation in Section A.2; for more details, see [31].

5.3. BRDF treatment

A scalar 3-kernel bidirectional reflectance distribution function (BRDF) scheme was implemented in LIDORT [32]. The scalar BRDF $\rho_{\mathrm{total}}(\mu,\mu',\phi-\phi')$ is specified as a linear combination of (up to) three

semi-empirical kernel functions:

$$\rho_{\text{total}}(\mu,\mu',\phi-\phi') = \sum_{k=1}^{3} R_k \rho_k(\mu,\mu',\phi-\phi';\mathbf{b}_k). \tag{98}$$

Here, R_k are the kernel amplitudes. For each kernel BRDF ρ_k, the geometrical dependence is known, but the function depends on vector $\mathbf{b}_k$ of pre-specified parameters. A well-known example is the Cox–Munk BRDF for glitter reflectance from the ocean [64]; this is a combination of a wave-facet probability distribution function (depending on wind-speed W), and a Fresnel reflection function (depending on the air–water relative refractive index m_{rel}). In this case, vector $\mathbf{b}_k$ has two elements: $\mathbf{b}_k = \{W, m_{\text{rel}}\}$. For a Lambertian surface, there is only one kernel: $\rho_1 \equiv 1$ for all incident and reflected angles, and coefficient R_1 is just the Lambertian albedo.

In order to develop solutions in terms of a Fourier azimuth series, Fourier components are calculated through:

$$\rho_k^m(\mu,\mu';\mathbf{b}_k) = \frac{1}{2\pi}\int_0^{2\pi} \rho_k(\mu,\mu',\phi;\mathbf{b}_k)\cos m\phi \,\mathrm{d}\phi. \tag{99}$$

This integration over the azimuth angle from zero to 2π is done by numerical quadrature; the number of BRDF azimuth quadrature abscissa N_{BRDF} is set to 50 to obtain a numerical accuracy of 10^{-4} for all kernels considered in [32]. Linearization of this BRDF scheme was reported in [32], and a mechanism developed for the generation of surface property weighting functions with respect to the kernel amplitudes R_k and also to elements of the non-linear kernel parameters $\mathbf{b}_k$.

In VLIDORT, the BRDF is actually a 4×4 matrix linking incident and reflected Stokes 4-vectors (cf. boundary condition (III) in Section 2.3). The scalar BRDF scheme outlined above has been fully implemented in VLIDORT by setting the {1,1} element of a 4×4 vector kernel ρ_k equal to the corresponding scalar kernel function ρ_k; all other elements are zero. However, a non-trivial vector kernel function for sea-surface glitter reflectance has been implemented in VLIDORT. This is based on the specification in [41]; further vector BRDF implementations are currently being researched. We make one remark here concerning post-processing of the radiation field in the presence of BRDF surfaces.

For non-Lambertian surfaces, the reflected radiation field is the sum of diffuse and direct components for each Fourier term. One can compute the direct reflected beam with a precise set of BRDF kernels rather than use their truncated forms based on a (finite) Fourier series expansion (M. Christi, private communication). This exact "direct beam (DB) correction" is done before the diffuse field calculation (Fourier convergence of the whole field is discussed in Section 6.3). The only additional requirement is for an exact computation of the derivatives of this DB correction with respect to the kernel amplitudes and parameters. For atmospheric weighting functions, the solar beam transmittance that forms part of the DB correction also needs to be differentiated with respect to variables ξ_p varying in layer p.

6. The numerical VLIDORT model

6.1. Summary of model capability

VLIDORT Version 2.0 has the following attributes:

- Pseudo-spherical solar beam attenuation, including refractive geometry;
- output at Arbitrary viewing geometry and optical depth output;
- downwelling and/or upwelling output;
- flux and mean-intensity output options;
- multi-solar beam output;–-Tanaka) correction, direct-beam correction;
- complete kernel-model BRDF implementation for scalar reflection;
- enhanced performance elements (solution-saving modes).

Linearization capabilities installed in Version 2.0 are:

- Complete output of atmospheric property weighting functions for upwelling and downwelling directions, at arbitrary viewing geometry and optical depths.
- Surface property weighting functions for all BRDF scalar-kernel parameters.
- Linearization of Delta-M treatment, single scatter and direct-beam corrections.
- Weighting functions for flux and mean intensity.
- Linearization of enhanced performance elements.

In this chapter we discuss aspects of the numerical model, including the preparation of optical property inputs (Section 6.2), benchmarking (6.3) and performance enhancements (Section 6.4).

6.2. Preparation of inputs

6.2.1. Optical property inputs

As an example, we consider a medium with Rayleigh scattering by air molecules, some trace gas absorption, and scattering and extinction by aerosols. If the Rayleigh scattering optical thickness is δ_{Ray}, the trace gas absorption optical thickness is δ_{gas}, and the aerosol extinction and scattering optical depths are τ_{aer} and δ_{aer}, respectively, then the total optical property inputs are given by

$$\Delta = \alpha_{\mathrm{gas}} + \delta_{\mathrm{Ray}} + \tau_{\mathrm{aer}}; \quad \omega = \frac{\delta_{\mathrm{aer}} + \delta_{\mathrm{Ray}}}{\Delta} \quad \mathbf{B}_l = \frac{\delta_{\mathrm{Ray}}\mathbf{B}_{l,\mathrm{Ray}} + \delta_{\mathrm{aer}}\mathbf{B}_{l,\mathrm{aer}}}{\delta_{\mathrm{Ray}} + \delta_{\mathrm{aer}}}. \tag{100}$$

The set of "Greek constants" for Rayleigh scattering are shown in Table 1 in terms of the depolarization ratio ρ [48]. Aerosol quantities must be derived from a model of electromagnetic scattering by particles (Mie calculations, T-matrix methods, etc.). See the remarks after Eq. (14) in Section 2.1.

Consider now the linearized optical property inputs (Eq. (33)) for this example. We suppose there is a single absorbing gas, with C the layer partial column, and σ_{gas} the column absorption coefficient, so that $\alpha_{\mathrm{gas}} = C\sigma_{\mathrm{gas}}$ in Eq. (100). For trace gas profile Jacobians, we require the derivatives in Eq. (33) as inputs, taken with respect to C. These are:

$$\mathscr{V}_C \equiv C\frac{\partial \Delta}{\partial C} = C\sigma_{\mathrm{gas}}; \quad \mathscr{U}_C \equiv C\frac{\partial \omega}{\partial C} = -\frac{\omega C\sigma_{\mathrm{gas}}}{\Delta}; \quad \mathscr{L}_{l,C} \equiv C\frac{\partial \mathbf{B}_l}{\partial C} = 0. \tag{101}$$

6.2.2. Additional inputs

For the pseudo-spherical calculation, we require atmospheric slant path distances for attenuation in a curved atmosphere. To compute this geometrical information, we need the Earth's radius R_{earth} and a height grid $\{z_n\}$ running from $n = 0$ to $n = N_{\mathrm{TOTAL}}$ (the total number of layers); heights are specified at layer boundaries with z_0 at TOA. This information is sufficient for straight-line paths. If the atmosphere is refracting, one must specify pressure and temperature fields $\{p_n\}$ and $\{t_n\}$, also defined at layer boundaries. The refractive geometry calculation inside VLIDORT is based on the Born–Wolf approximation for refractive index $r(z)$ as a function of height: $r(z) = 1 + \alpha_0 p(z)/t(z)$. Factor α_0 depends slightly on wavelength, but to a very good approximation, it is 0.000288 multiplied by the air density at standard temperature and pressure.

Table 1
Greek matrix coefficients for Rayleigh scattering

	α_L	β_L	γ_L	δ_L	ε_L	ζ_L
$l=0$	0	1	0	0	0	0
$l=1$	0	0	0	$\frac{3(1-2\rho)}{2+\rho}$	0	0
$l=2$	$\frac{6(1-\rho)}{2+\rho}$	$\frac{(1-\rho)}{2+\rho}$	$-\frac{\sqrt{6}(1-\rho)}{2+\rho}$	0	0	0

From Section 5.3, for BRDF input, one must specify up to three kernel amplitudes coefficients $\{R_k\}$ and the corresponding vectors $\{\mathbf{b}_k\}$. Lambertian surfaces are a special case: the BRDF formalism is bypassed and the only input is a Lambertian albedo. For surface-property Jacobians, no additional inputs are needed other than control flags.

6.2.3. Reducing the number of jacobians

In the above example, we could define five weighting functions with respect to δ_{Ray}, τ_{aer}, δ_{aer}, C and σ_{gas} and set VLIDORT to calculate all these quantities in separate computations. However, we can reduce this number by calculating Jacobians only with respect to the basic optical inputs, and then combining results with the chain rule. Any desired weighting functions can be expressed in terms of a more basic set based on the input optical properties (E. Ustinov, private communication). For example, we could write for the trace gas quantities:

$$\frac{\partial I}{\partial C}=\frac{\partial I}{\partial \Delta}\frac{\partial \Delta}{\partial C}+\frac{\partial I}{\partial \omega}\frac{\partial \omega}{\partial C}=\left(\frac{\partial I}{\partial \Delta}-\frac{\partial I}{\partial \omega}\frac{\omega}{\Delta}\right)\sigma_{\mathrm{gas}}, \tag{102}$$

$$\frac{\partial I}{\partial \sigma_{\mathrm{gas}}}=\frac{\partial I}{\partial \Delta}\frac{\partial \Delta}{\partial \sigma_{\mathrm{gas}}}+\frac{\partial I}{\partial \omega}\frac{\partial \omega}{\partial \sigma_{\mathrm{gas}}}=\left(\frac{\partial I}{\partial \Delta}-\frac{\partial I}{\partial \omega}\frac{\omega}{\Delta}\right)C. \tag{103}$$

From these two results, we see that Jacobians for the partial column amount and absorber cross-section are proportional; only one of two needs to be calculated. The question of proportionality between weighting functions was investigated in detail in the context of ozone profile retrieval from space using LIDORT as the forward model [30]. Although it is possible to work only with the basic optical property Jacobians, we have maintained flexibility for VLIDORT: it is up to the user to define linearized optical property inputs.

We make one final remark concerning bulk property Jacobians. An atmospheric profile may depend on a single quantity—for example, a climatology of ozone profiles $\{U_n\}$ based on a classification by total ozone column C [65]. In this case, each profile entry $U_n(C)$ is parameterized in terms of C, and the total column Jacobian is the chain-rule sum:

$$\frac{\partial I}{\partial C}=\sum_{n=1}^{N_{\mathrm{TOTAL}}}\frac{\partial I}{\partial U_n}\frac{\partial U_n}{\partial C}. \tag{104}$$

On the face of it, Eq. (104) requires N_{TOTAL} profile weighting function computations and an external summation. It is actually possible to adjust the linearized optical property inputs and perform the summation in Eq. (104) *inside* the scattering code, thus reducing the number of Jacobian calculations from N_{TOTAL} to 1. This "bulk property" linearization has been implemented in the scalar LIDORT code form some applications, and is under construction for VLIDORT.

6.3. Validation and benchmarking

6.3.1. Checking against the scalar code

VLIDORT is designed to work equally with Stokes 4-vectors $\mathbf{I}=\{I, Q, U, V\}$ and in scalar mode (I only). A first validation is to run VLIDORT in scalar mode and reproduce results generated independently with LIDORT. One can test the major functions of the model (the real RT solutions, the boundary value problem and post-processing) for a representative range of scenarios (single layer, multilayer, arbitrary optical thickness and viewing angle output, plane-parallel versus pseudo-spherical, etc.). This battery of scalar-only tests is very useful, but of course, it does not validate the 4-vector solutions. Verification of the boundary value problem and multilayer capability is tested using the invariance principle: for a slab comprising two identical layers of optical thickness values τ_1 and τ_2, the slab reflectance (at least for plane-parallel geometry) is identical to that produced by a single layer with the same scattering properties but with optical thickness $\tau_1+\tau_2$. This applies equally to the scalar and vector models.

6.3.2. The rayleigh slab problem

A validation was carried out against results published in the tables of Coulson, Dave and Sekera (CDS) [2]. This is a single-layer Rayleigh medium in plane-parallel geometry; the single scattering albedo is 1.0 and there is no depolarization in the scattering matrix. CDS tables for Stokes parameters I, Q and U are given for three surface albedos (0.0, 0.25, 0.80), a range of optical thickness values from 0.01 to 1.0, for 7 azimuths from 0° to 180° at 30° intervals, some 16 view zenith angles with cosines from 0.1 to 1.0, and for 10 solar zenith angles with cosines from 0.1 to 1.0. With the single scattering albedo set to 0.999999, VLIDORT was able to reproduce all these results to within the levels of accuracy specified in the tables.

6.3.3. Benchmarking for aerosol slab problems

We first consider benchmark results noted in [19]. The slab problem used a solar angle 53.130° ($\mu_0 = 0.6$), with single scatter albedo $\omega = 0.973527$, surface albedo 0.0, total layer optical thickness of 1.0, and a set of Greek constants as noted in Table 1 of [19]. 24 discrete ordinate streams were used in the half space. With one exception discussed below, all results in [19] were reproduced by VLIDORT, with numerical differences of 1 or 2 in the sixth decimal place. In Table 2, we present VLIDORT results for intensity I at relative azimuth 180°; the format is deliberately chosen to mimic that in [19]. It is clear that the agreement with Table 8 in [19] is almost perfect. The only departure is the downwelling output at $\mu = 0.6$: this is a limiting case because $\mu_0 = 0.6$ as well. To avoid singularities in the limit as $\mu \to \mu_0$, a small-numbers analysis has been implemented in VLIDORT (as also in LIDORT); this issue was not discussed in [19].

An additional benchmarking for VLIDORT has been done against the results of Garcia and Siewert [10] for a similar slab problem, this time with surface albedo 0.1. With VLIDORT set to calculate with 20 discrete ordinate streams, Tables 3–10 in [10] were reproduced to within one digit of six significant figures. This result is noteworthy because the radiative transfer computations in [10] were done using a completely different methodology (the "F_N" method).

6.3.4. Weighting function verification

It is usually sufficient to validate Jacobians with finite difference estimates. If Stokes vector result $\mathbf{I}$ is obtained with parameter ξ, and (all other inputs being equal) another Stokes vector $\mathbf{I}'$ obtained with perturbed

Table 2
Replica of Table 8 from Siewert [19]

	0.000	0.125	0.250	0.500	0.750	0.875	1.000
−1.0	5.06872E-02	4.26588E-02	3.45652E-02	1.97273E-02	7.87441E-03	3.36768E-03	
−0.9	4.49363E-02	3.83950E-02	3.16314E-02	1.87386E-02	7.81148E-03	3.42290E-03	
−0.8	4.95588E-02	4.29605E-02	3.59226E-02	2.19649E-02	9.46817E-03	4.21487E-03	
−0.7	5.54913E-02	4.89255E-02	4.16034E-02	2.63509E-02	1.18019E-02	5.35783E-03	
−0.6	6.19201E-02	5.57090E-02	4.83057E-02	3.18640E-02	1.49296E-02	6.94694E-03	
−0.5	6.84108E-02	6.30656E-02	5.59610E-02	3.87231E-02	1.91563E-02	9.19468E-03	
−0.4	7.44303E-02	7.06903E-02	6.44950E-02	4.72940E-02	2.50375E-02	1.25100E-02	
−0.3	7.89823E-02	7.78698E-02	7.35194E-02	5.79874E-02	3.35858E-02	1.77429E-02	
−0.2	8.01523E-02	8.29108E-02	8.16526E-02	7.07286E-02	4.66688E-02	2.69450E-02	
−0.1	7.51772E-02	8.29356E-02	8.56729E-02	8.26216E-02	6.65726E-02	4.61143E-02	
−0.0	5.93785E-02	7.61085E-02	8.33482E-02	8.76235E-02	8.22105E-02	7.53201E-02	
0.0		7.61085E-02	8.33482E-02	8.76235E-02	8.22105E-02	7.53201E-02	6.04997E-02
0.1		4.81348E-02	7.00090E-02	8.63151E-02	8.80624E-02	8.49382E-02	7.76333E-02
0.2		2.95259E-02	5.13544E-02	7.72739E-02	8.77078E-02	8.84673E-02	8.55909E-02
0.3		2.07107E-02	3.91681E-02	6.67896E-02	8.29733E-02	8.70779E-02	8.79922E-02
0.4		1.58301E-02	3.14343E-02	5.81591E-02	7.72710E-02	8.36674E-02	8.74252E-02
0.5		1.28841E-02	2.64107E-02	5.17403E-02	7.22957E-02	8.01999E-02	8.60001E-02
0.6		1.10823E-02	2.32170E-02	4.74175E-02	6.88401E-02	7.78121E-02	8.51316E-02
0.7		1.01614E-02	2.15832E-02	4.53651E-02	6.77032E-02	7.75916E-02	8.61682E-02
0.8		1.03325E-02	2.19948E-02	4.67328E-02	7.07013E-02	8.16497E-02	9.14855E-02
0.9		1.31130E-02	2.72721E-02	5.64095E-02	8.41722E-02	9.68476E-02	1.08352E-01
1.0		4.54878E-02	8.60058E-02	1.53099E-01	2.03657E-01	2.23428E-01	2.39758E-01

input $\xi' = \xi(1+\varepsilon)$ for some small number ε, then the normalized Jacobian is approximated by:

$$\mathbf{K}_\xi \equiv \xi \frac{\partial \mathbf{I}}{\partial \xi} \approx \xi \frac{\delta \mathbf{I}}{\delta \xi} = \frac{\delta \mathbf{I}}{\varepsilon} = \frac{(\mathbf{I}' - \mathbf{I})}{\varepsilon}. \tag{105}$$

Verification of each stage of the linearization process may also be done in this way. For RT models without linearization, it is of course always possible to attempt weighting function estimations using finite-difference methods. However, there are pitfalls associated with this procedure (quite apart from the arbitrariness and time-consuming nature of the exercise). In certain situations, a small perturbation of one or more of the Greek constants can give rise to a set of eigensolutions which cannot be compared (in a finite-difference sense) with those generated with the original unperturbed inputs.

6.4. Performance considerations

6.4.1. Multiple solar zenith angle facility

VLIDORT has the capability to handle multiple solar zenith angles (SZAs). In the numerical model, the most time-consuming tasks are the determination of the homogeneous equation eigensolutions and the generation of the inverse (by LU decomposition) of the BVP matrix. Both these tasks are independent of solar source terms, and they can be performed for each Fourier component before solar terms are computed. Once done, the internal SZA loop in VLIDORT performs repeated determinations of particular integrals, followed by corresponding BVP back-substitutions and post-processing. This represents a substantial performance improvement over a model that must be called repeatedly for each new SZA input. This is especially relevant for VLIDORT in view of the time taken over the eigenproblem (finding complex roots is more time-consuming) and the much larger BVP matrix inversion compared with that for the scalar code. The multiple SZA facility is particularly useful for look-up table generation: a single call to VLIDORT will generate output for a complete range of solar and satellite viewing geometries.

6.4.2. Convergence of the fourier cosine/sine azimuth series

In VLIDORT, the exact single scatter term is computed *before* the discrete ordinate calculation of the diffuse field. (In earlier LIDORT versions, this term was calculated after the diffuse field computation). The single scatter Stokes intensity and Jacobian fields are computed at all output optical depths and then added to the respective Fourier $m = 0$ components of the diffuse field. VLIDORT will converge quickly, since higher-order Fourier components of the diffuse intensity are comparatively smaller when compared with the total field (M. Christi, private communication, see also [66]).

6.4.3. Eigensolver usage

In Sections 3.1 and 3.2, we noted some differences between the LAPACK solver DGEEV and the ASYMTX package as used in the LIDORT and DISORT models. Aside from additional elements along the diagonal, the eigenmatrix $\tilde{\mathbf{\Gamma}}_n$ in layer n consists of blocks of 4×4 matrices of the form $\mathbf{P}_{lm}(\mu_i)\mathbf{B}_{nl}\mathbf{P}_{lm}^{\mathrm{T}}(\mu_j)$ (Eq. (40)). Since $\mathbf{P}$ and $\mathbf{P}^{\mathrm{T}}$ are symmetric, then each such 4×4 matrix will be symmetric if $\mathbf{B}_{nl}$ has this property. This is the case if the "Greek constant" ε_{nl} in $\mathbf{B}_{n\mathrm{l}}$ is zero for all values of l. When this condition holds, the eigenmatrix can be transformed into a symmetric matrix. Eigensolutions are then real-valued and may be obtained using the ASYMTX solver. This special case is satisfied by the Rayleigh scattering law, but does not hold for scattering with aerosols and clouds. In the latter case, the lack of symmetry will lead to complex roots and the need for the DGEEV eigensolver. Conversely, for Rayleigh scattering we can use the faster "real-only" ASYMTX package. The policy in VLIDORT is to retain both eigensolvers and use them as required—if ε_{nl} is non-zero in layer n, then we choose DGEEV, if zero, then ASYMTX.

6.4.4. Solution saving and BVP telescoping

Four-vector codes are computationally slower, nominally by a factor of $\sim$16 compared with scalar codes, and the use of complex eigensolvers further slows the models. Codes can be made faster by implementing timesaving devices, and here, VLIDORT has two performance enhancements.

The first is "solution saving". For Fourier component m, if there is no scattering in layer n, then the RTE solution is trivial: Beer-Lambert extinction with solutions $\mathbf{I}(x,\mu) = \mathbf{I}(0,\mu)\exp[-x/\mu]$ for any stream direction μ. Thus, for N discrete ordinates μ_j in the half-space, the homogeneous solution eigenvector $\tilde{\mathbf{X}}_\alpha$ (size 4N) has zero entries apart from four diagonal elements corresponding to the 4×4 matrix $\mathbf{D} = diag\{1,1,-1,-1\}$ for discrete ordinate $j=\alpha$. There is no need to invoke the eigensolver. There is no solar source term and hence no particular solution computation. For post-processing, source function integration is a simple transmittance recursion. In general, when all six Greek coefficients are zero for $m \leqslant 1 \leqslant 2N-1$, then there is no scattering for Fourier components m and higher, and solution saving applies. Rayleigh scattering has a $\cos^2\Theta$ phase matrix dependency on scattering angle Θ, with no molecular scattering for Fourier components $m>2$. Thus, in a "mostly Rayleigh" atmosphere with a small number of aerosol layers, solution saving can lead to considerable savings in CPU time.

The second enhancement is "BVP Telescoping". We consider an atmosphere with Rayleigh scattering everywhere, except for a block of contiguous layers containing both Rayleigh and particulate scatterers. For Fourier $m>2$, the solution saving enhancement will apply. Homogeneous and particular solutions are only present in the block of contiguous layers, so that the boundary value problem can then be "telescoped" to compute only those constants of integration for this block of mixed-scatterer layers. Constants of integration in the non-active layers (where there is no scattering) are then found by propagating the block results using transmittance factors. An exposition of the telescoped BVP is in Appendix B.

7. Concluding remarks

In this paper, we have described the multilayer multiple scattering vector discrete ordinate radiative transfer model VLIDORT. The vector RTE has both complex variable and real-value solutions. The model has a fully linearized pseudo-spherical capability to deal with solar beam attenuation in a curved atmosphere. We have focused in particular on the linearization capacity of the model: the ability to generate analytic weighting functions of the Stokes field with respect to any atmospheric or surface parameter. We have also discussed the implementation of exact single scatter calculations (including linearizations). The model has been validated against a number of benchmarks in the literature. We have discussed a number of performance aspects, including the multiple SZA facility, and the use of timesaving devices such as solution saving.

VLIDORT Version 2.0 has all the capabilities of its scalar counterpart LIDORT Version 3.0. Both codes have been streamlined and reorganized so that inputs and outputs are consistent. VLIDORT Version 2.0 is available on the RT Solutions web site at www.rtslidort.com. A User's Guide and a GNU-type public license accompany this release of the code. LIDORT Version 3.0 is also available from this source.

Acknowledgments

The author would like to thank Jukaa Kujanpaa (Finnish Meteorological Institute) and Vijay Natraj (CalTech) for some very helpful user feedback. Radiative transfer colleagues Mick Christi (Colorado State University) and Knut Stamnes (Stevens Institute for Technology) are also acknowledged for a number of stimulating discussions. Discussions with Nick Krotkov and Eugene Ustinov are also appreciated.

The main source of funding for the VLIDORT development came from two Ozone SAF Visiting Scientist Grants (FMI, Finland). Part of the research described in this paper was performed for the Orbiting Carbon Observatory Project at the Jet Propulsion Laboratory, California Institute of Technology, under contracts with the National Aeronautics and Space Administration.

Appendix A. Spherical corrections

A.1. Pseudo-spherical approximation

The P-S approximation assumes solar beam attenuation for a curved atmosphere. The approximation is a standard feature of many radiative transfer models. We follow the formulation in [29]. Fig. 2 provides geometrical sketches appropriate to both sections of this appendix.

We consider a stratified atmosphere of optically uniform layers, with extinction optical depths $\{\Delta_n\}$, $n = 1$, N_{TOTAL} (the total number of layers). We take points V_{n-1} and V_n on the vertical (Fig. 2, upper panel), and the respective solar beam transmittances to these points are then:

$$T_{n-1} = \exp\left[-\sum_{k=1}^{n-1} s_{n-1,k}\Delta_k\right]; \quad T_n = \exp\left[-\sum_{k=1}^{n} s_{n,k}\Delta_k\right]. \tag{A.1}$$

Here, $s_{n,k}$ is the path distance geometrical factor (Chapman factor), equal to the path distance covered by the V_n beam as it traverses through layer k divided by the corresponding vertical height drop (geometrical thickness of layer k). At the top of the atmosphere, $T_0 = 1$. In the *average secant* parameterization, the transmittance to any intermediate point between V_{n-1} and V_n is parameterized by:

$$T(x) = T_{n-1}\exp[-\lambda_n x], \tag{A.2}$$

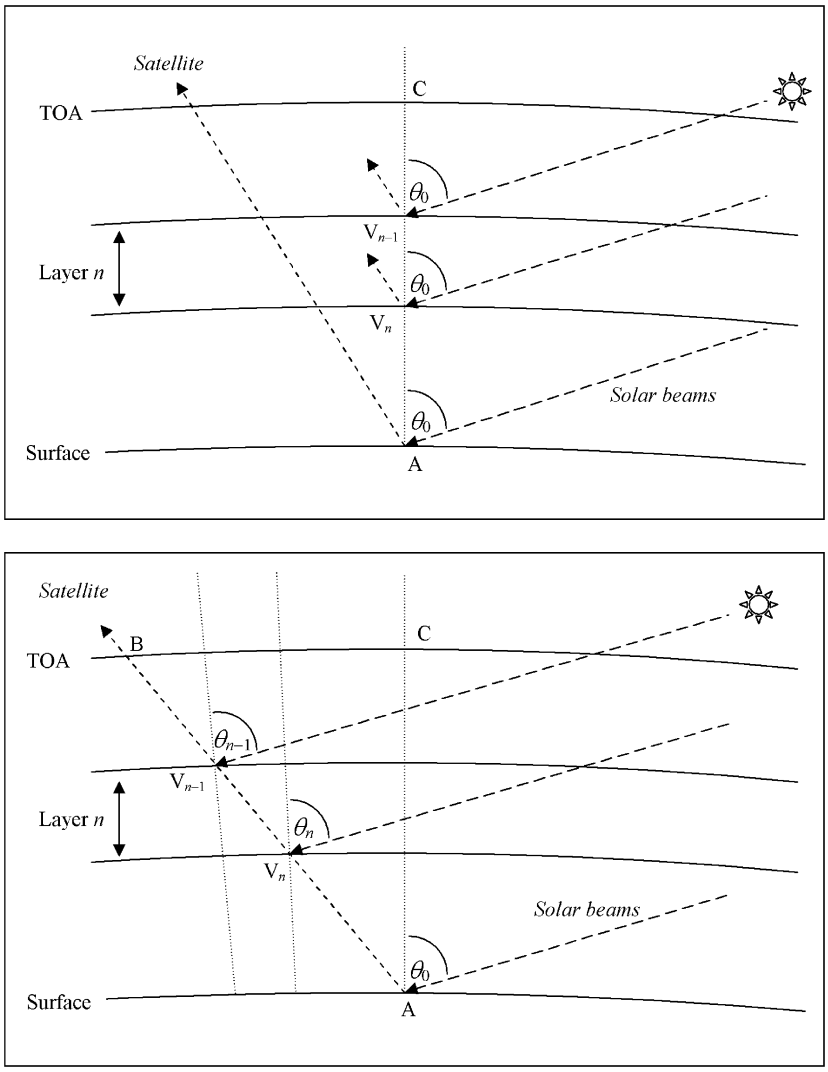

Fig. 2. (Upper panel) Pseudo-spherical viewing geometry for scattering along the zenith. (Lower panel) Line of sight path AB in a curved atmosphere, with viewing and solar angles changing along the path from A to B.

where x is the vertical optical thickness measured downwards from V_{n-1} and λ_n the average secant for this layer. Substituting (A.2) into (A.1) and setting $x = \Delta_n$ we find:

$$\lambda_n = \frac{1}{\Delta_n}\left[\sum_{k=1}^{n} s_{n,k}\Delta_k - \sum_{k=1}^{n-1} s_{n-1,k}\Delta_k\right]. \tag{A.3}$$

In the plane-parallel case, we have $\lambda_n = \mu_0^{-1}$ for all n.

Linearization: We require derivatives with respect to an atmospheric property ξ_k in layer k. The basic linearized optical property input is the normalized derivative V_n of the layer optical depth extinction Δ_n (Eq. (33)). Applying the linearization operator to (A.3) and (A.1), we find:

$$\mathscr{L}_k[\lambda_n] = \frac{\mathscr{V}}{\Delta_n}\left(s_{n,n} - \lambda_n\right), \quad \mathscr{L}_k[T_n] = 0, \quad (k = n), \tag{A.4}$$

$$\mathscr{L}_k[\lambda_n] = \frac{\mathscr{V}_k}{\Delta_n}\left(s_{n,k} - s_{n-1,k}\right), \quad \mathscr{L}_k[T_n] = -\mathscr{V}_k s_{n-1,k} T_n; \quad (k<n), \tag{A.5}$$

$$\mathscr{L}_k[\lambda_n] = 0; \quad \mathscr{L}_k[T_n] = 0; \quad (k>n). \tag{A.6}$$

For the plane-parallel case, we have:

$$\mathscr{L}_k[\lambda_n] = 0\ (\forall k, \forall n); \quad \mathscr{L}_k[T_n] = -\frac{\mathscr{V}_k T_n}{\mu_0}(k<n); \quad \mathscr{L}_k[T_n] = 0 \quad (k \geqslant n). \tag{A.7}$$

A.2. Sphericity along the line-of-sight

In the previous section, scattering was assumed to take place along the nadir, so that the scattering geometry $\Omega \equiv \{\mu_0, \mu, \phi - \phi_0\}$ is unchanged along the vertical. For a slant line-of-sight path (Fig. 2, lower panel), the scattering geometry varies along the path. For layer n traversed by this path, the upwelling Stokes vector at the layer-top is (to a high degree of accuracy) given by:

$$\mathbf{I}^{\uparrow}(\Omega_{n-1}) \cong \mathbf{I}^{\uparrow}(\Omega_n)T(\Omega_n) + \mathbf{\Lambda}_n^{\uparrow}(\Omega_n) + \mathbf{M}_n^{\uparrow}(\Omega_n). \tag{A.8}$$

Here, $\mathbf{I}^{\uparrow}(\Omega_n)$ is the Stokes vector at the layer bottom, $T(\Omega_n)$ the layer transmittance along the line of sight, and $\mathbf{\Lambda}_n^{\uparrow}(\Omega_n)$ and $\mathbf{M}_n^{\uparrow}(\Omega_n)$ are the single- and multiple-scatter layer 4-vector source terms, respectively. The transmittance and layer source terms are evaluated with scattering geometry Ω_n at position V_n. Equation (A.8) is applied recursively, starting with the upwelling Stokes vector $\mathbf{I}_{\mathrm{BOA}}^{\uparrow}(\Omega_{N_{\mathrm{TOTAL}}})$ evaluated at the surface for geometry $\Omega_{N_{\mathrm{TOTAL}}}$, and finishing with the Stokes field at top of atmosphere ($n = 0$). The transmittances and single-scatter layer source terms may be determined through an accurate single scatter calculation (cf. Eq. (97)) allowing for changing geometrical angles along the line of sight. To evaluate the multiple scatter sources, we run VLIDORT in "multiple-scatter mode" successively for each of the geometries from $\Omega_{N_{\mathrm{TOTAL}}}$ to Ω_1, retaining only the appropriate multiple scatter layer source terms, and, for the first VLIDORT calculation with the lowest-layer geometry $\Omega_{N_{\mathrm{TOTAL}}}$, the surface upwelling Stokes vector $\mathbf{I}_{\mathrm{BOA}}^{\uparrow}(\Omega_{N_{\mathrm{TOTAL}}})$.

For N_{TOTAL} layers in the atmosphere, we require N_{TOTAL} separate calls to VLIDORT, and this is much more time consuming that a single P-S call with geometry $\Omega_{N_{\mathrm{TOTAL}}}$ (this would be the default in the absence of a line-of-sight correction). However, since scattering is strongest near the surface, the first VLIDORT call (with geometry $\Omega_{N\mathrm{TOTAL}}$) is the most important as it provides the largest scattering source term $\mathbf{M}_{N_{\mathrm{TOTAL}}}^{\uparrow}(\Omega_{N_{\mathrm{TOTAL}}})$. An even simpler line-of-sight correction is to assume that *all* multiple scatter source terms are taken from this first VLIDORT call; in this case, we require only the accurate single scatter calculation to complete $\mathbf{I}_{\mathrm{TOA}}^{\uparrow}$. This approximation is known as the "poor man's" sphericity correction; it requires very little extra computational effort compared to a single call with the regular P-S geometry. The sphericity correction can also be set up with just two calls to VLIDORT made with the start and finish geometries $\Omega_{N_{\mathrm{TOTAL}}}$ and Ω_1; in this case, multiple scatter source terms at other geometries are *interpolated* at all levels between results obtained for the two limiting geometries. Accuracies for these corrections were investigated in [31] for the scalar code; results for VLIDORT are similar.

Appendix B. Boundary value problem telescoping

The exposition below is given for scalar RT, but the same principles apply to the vector model; the bookkeeping is more complicated. The discrete ordinate solution for layer n may be written:

$$I_n^{\pm}(x,\mu_i) = \sum_{\alpha=1}^{N}\left[L_{n\alpha}X_{in\alpha}^{\pm}\mathrm{e}^{-k_{n\alpha}x} + M_{n\alpha}X_{in\alpha}^{\mp}\mathrm{e}^{-k_{n\alpha}(\Delta_n-x)}\right] + G_{in}^{\pm}\exp[-\lambda_n x]. \tag{B.1}$$

Let us assume now that n is a single "active" layer containing aerosol scatterers in what is otherwise a Rayleigh atmosphere with N_{TOTAL} layers. When solution saving (Section 6.4) is in place, then $X_{ip\alpha}^{\pm} = \delta_{i\alpha}$ and $G_{ip}^{\pm} = 0$ for all Fourier components $m > 2$ and for all layers $p \neq n$. Thus for non-active layers, the downwelling and upwelling solutions are:

$$I_{pj}^{+}(x) = L_{pj}\exp[-x/\mu_j]; \quad I_{pj}^{-}(x) = M_{pj}\exp[-(\Delta_p - x)/\mu_j]. \tag{B.2}$$

Boundary value constants propagate upwards and downwards through non-active layers via:

$$L_{p+1,j} = L_{pj}\exp[-\Delta_p/\mu_j]; \quad M_{p-1,j} = M_{pj}\exp[-\Delta_p/\mu_j]. \tag{B.3}$$

If we can find BVP coefficients $\{L_{n\alpha}, M_{n\alpha}\}$ for the active layer n, then coefficients for all other layers will follow by propagation. At the top of layer n, the boundary condition is:

$$\sum_{\alpha=1}^{N}\left[L_{n\alpha}X_{in\alpha}^{+} + M_{n\alpha}X_{in\alpha}^{-}\Theta_{n\alpha}\right] + G_{in}^{+} = L_{n-1,i}C_{n-1,i}, \tag{B.4}$$

$$\sum_{\alpha=1}^{N}\left[L_{n\alpha}X_{in\alpha}^{-} + M_{n\alpha}X_{in\alpha}^{+}\Theta_{n\alpha}\right] + G_{in}^{-} = M_{n-1,i}. \tag{B.5}$$

At the bottom of this active layer, the boundary condition is:

$$\sum_{\alpha=1}^{N}\left[L_{n\alpha}X_{in\alpha}^{+}\Theta_{n\alpha} + M_{n\alpha}X_{in\alpha}^{-}\right] + G_{in}^{+}\Lambda_{n\alpha} = L_{n+1,i}, \tag{B.6}$$

$$\sum_{\alpha=1}^{N}\left[L_{n\alpha}X_{in\alpha}^{-}\Theta_{n\alpha} + M_{n\alpha}X_{in\alpha}^{+}\right] + G_{in}^{-}\Lambda_{n\alpha} = M_{n+1,i}C_{n+1,j}. \tag{B.7}$$

We have used the following abbreviations:

$$\Theta_{n\alpha} = \exp[-k_{n\alpha}\Delta_n]; \quad \Delta_n = \exp[-\lambda_n\Delta_n]; \quad C_{nj} = \exp[-\Delta_n/\mu_j]. \tag{B.8}$$

We now consider the top and bottom of atmosphere boundary conditions. At TOA, there is no diffuse radiation, so that $L_{p\alpha} = 0$ for $p = 1$ and hence by Eq. (B.3) for all $1 < p < n$. At the surface, the Lambertian reflection condition only applies for Fourier $m = 0$; for any other component, there is no reflection, and so $M_{p\alpha} = 0$ for $p = N_{\mathrm{TOTAL}}$ and hence by Eq. (B.3) for all $N_{\mathrm{TOTAL}} > p > n$. Eqs. (B.4) and (B.7) then become:

$$\sum_{\alpha=1}^{N}\left[L_{n\alpha}X_{in\alpha}^{+} + M_{n\alpha}X_{in\alpha}^{-}\Theta_{n\alpha}\right] = -G_{in}^{+}, \tag{B.9}$$

$$\sum_{\alpha=1}^{N}\left[L_{n\alpha}X_{in\alpha}^{-}\Theta_{n\alpha} + M_{n\alpha}X_{in\alpha}^{+}\right] = -G_{in}^{-}\Lambda_{n\alpha}. \tag{B.10}$$

This is a system of rank $2N$ for the unknowns $\{L_{p\alpha}, M_{p\alpha}\}$ and is solved by usual means (there is no compression here). For the layer immediately above n, we use (B5) to find $M_{n-1,\alpha}$ and for the remaining layers

to TOA, we use the propagation rule (B.2). Similarly, for the layer immediately below n, we use (B.6) to find $L_{n+1,\alpha}$ and for the remaining layers to the ground, we again use the propagation rule (B.2). This process may be applied to situations with more general boundary conditions at TOA and BOA. For example, a BRDF will in general provide a relation between $L_{N\mathrm{TOTAL},\alpha}$ and $M_{N\mathrm{TOTAL},\alpha}$, from which a relation between $L_{n+1,\alpha}$ and $M_{n+1,\alpha}$ is established from the propagation rules. Then, (B.6) and (B.7) can be combined in one equation to replace (B.10).

Solution saving and BVP telescoping operations come together in a natural way when one uses layer adding to solve for the radiation field (instead of the BVP linear algebra methods). In the Radiant model [67], layer RTE solutions are determined by discrete ordinate methods. Solutions are then combined to generate layer reflection and transmission matrices $\mathbf{r}_n$ and $\mathbf{t}_n$, and source vectors $\mathbf{s}^{\pm}{}_n$. Invariant principles are then used to add these quantities on a layer-by-layer basis to the stack of multilayer reflection and transmission matrices $\mathbf{R}_n$ and $\mathbf{T}_n$, and source vectors $\mathbf{S}^{\pm}{}_n$, until values for the whole atmosphere have been assembled. In solution saving mode, $\mathbf{r}_n = 0$, $\mathbf{s}^{\pm}{}_n = 0$ and $\mathbf{t}_n$ is a diagonal matrix with entries C_{nj} as defined in Eq. (B.8). Stack building with these layer terms is straightforward. Linearization principles for the Radiant model can be found in [66].

References

[1] Chandrasekhar S. Radiative Transfer. New York: Dover Publications Inc.; 1960.
[2] Coulson K, Dave J, Sekera D. Tables related to radiation emerging from planetary atmosphere with Rayleigh scattering. Berkeley: University of California Press; 1960.
[3] Hovenier JW. Multiple scattering of polarized light in planetary atmospheres. Astron Astrophys 1971;13:7–29.
[4] Dave JV. Intensity and polarization of the radiation emerging from a plane-parallel atmosphere containing monodispersed aerosols. Appl Opt 1970;9:2673–84.
[5] Hansen JE, Travis LD. Light scattering in planetary atmospheres. Space Sci Rev 1974;16:527–610.
[6] Siewert CE. On the equation of transfer relevant to the scattering of polarized light. Astrophys J 1981;245:1080–6.
[7] Siewert CE. On the phase matrix basic to the scattering of polarized light. Astron Astrophys 1982;109:195–200.
[8] Vestrucci P, Siewert CE. A numerical evaluation of an analytical representation of the components in a Fourier decomposition of the phase matrix for the scattering of polarized light. JQSRT 1984;31:177–83.
[9] Garcia RDM, Siewert CE. A generalized spherical harmonics solution for radiative transfer models that include polarization effects. JQSRT 1986;36:401–23.
[10] Garcia RDM, Siewert CE. The F_N method for radiative transfer models that include polarization. JQSRT 1989;41:117–45.
[11] Hovenier JW, van der Mee CVM. Fundamental relationships relevant to the transfer of polarized light in a scattering atmosphere. Astron Astrophys 1983;128:1–16.
[12] de Rooij WA, van der Stap CCAH. Expansion of Mie scattering matrices in generalized spherical functions. Astron Astrophys 1984;131:237–48.
[13] de Haan JF, Bosma PB, Hovenier JW. The adding method for multiple scattering of polarized light. Astron Astrophys 1987;183:371–91.
[14] Stammes P, de Haan JF, Hovenier JW. The polarized internal radiation field of a planetary atmosphere. Astron Astrophys 1989;225:239–59.
[15] Wauben WMF, Hovenier JW. JQSRT 1992;47:491–500.
[16] Stamnes K, Tsay S-C, Wiscombe W, Jayaweera K. Numerically stable algorithm for discrete ordinate method radiative transfer in multiple scattering and emitting layered media. Appl Optics 1988;27:2502–9.
[17] Schulz FM, Stamnes K. Angular distribution of the Stokes vector in a plane-parallel vertically inhomogeneous medium in the vector discrete ordinate radiative transfer (VDISORT) model. JQSRT 2000;65:609–20.
[18] Siewert CE. A concise and accurate solution to Chandrasekhar's basic problem in radiative transfer. JQSRT 2000;64:109–30.
[19] Siewert CE. A discrete-ordinates solution for radiative transfer models that include polarization effects. JQSRT 2000;64:227–54.
[20] Barichello LB, Garcia RDM, Siewert CE. Particular solutions for the discrete-ordinates method. JQSRT 2000;64:219–26.
[21] Rodgers CD. Inverse methods for atmospheric sounding: theory and practice. Singapore: World Scientific Publishing Co. Pte. Ltd.; 2000.
[22] Rozanov V, Diebel D, Spurr R, Burrows J. GOMETRAN: radiative transfer model for the satellite project GOME, the plane-parallel version. J Geophys Res 1997;102:16683–95.
[23] Rozanov V, Kurosu T, Burrows J. Retrieval of atmospheric constituents in the UV-visible: a new quasi-analytical approach for the calculation of weighting functions. JQSRT 1998;60:277–99.
[24] Ustinov EA. Analytic evaluation of the weighting functions for remote sensing of blackbody planetary atmospheres: a general linearization approach. JQSRT 2002;74:683–6.
[25] Ustinov EA. Atmospheric weighting functions and surface partial derivatives for remote sensing of scattering planetary atmospheres in thermal spectral region: general adjoint approach. JQSRT 2005;92:351–71.

[26] Landgraf J, Hasekamp O, Trautmann T, Box M. A linearized radiative transfer model for ozone profile retrieval using the analytical forward-adjoint perturbation theory approach. J Geophys Res 2001;106:27291–306.
[27] Hasekamp OP, Landgraf J. A linearized vector radiative transfer model for atmospheric trace gas retrieval. JQSRT 2002;75: 221–38.
[28] Spurr RJD, Kurosu TP, Chance KV. A linearized discrete ordinate radiative transfer model for atmospheric remote sensing retrieval. JQSRT 2001;68:689–735.
[29] Spurr RJD. Simultaneous derivation of intensities and weighting functions in a general pseudo-spherical discrete ordinate radiative transfer treatment. JQSRT 2002;75:129–75.
[30] Van Oss RF, Spurr RJD. Fast and accurate 4- and 6-stream linearized discrete ordinate radiative transfer models for ozone profile retrieval. JQSRT 2002;75:177–220.
[31] Spurr RJD. LIDORT V2PLUS: a comprehensive radiative transfer package for UV/VIS/NIR nadir remote sensing; a general quasi-analytic solution. In: Proceedings of the SPIE International Symposium, Remote Sensing 2003, Barcelona, Spain, September 2003.
[32] Spurr RJD. A new approach to the retrieval of surface properties from earthshine measurements. JQSRT 2004;83:15–46.
[33] Mishchenko M, Lacis A, Travis L. Errors induced by the neglect of polarization in radiance calculations for Rayleigh scattering atmospheres. JQSRT 1994;51:491–510.
[34] Lacis A, Chowdhary J, Mishchenko M, Cairns B. Modeling errors in diffuse sky radiance: vector vs. scalar treatment. Geophys Res Lett 1998;25:135–8.
[35] Sromovsky LA. Effects of Rayleigh-scattering polarization on reflected intensity: a fast and accurate approximation method for atmospheres with aerosols. Icarus 2005;173:284.
[36] Schutgens N, Stammes P. A novel approach to the polarization correction of spaceborne spectrometers. J Geophys Res 2003;108:4229, doi:10.1029/2002JD002736.
[37] Hasekamp O, Landgraf J, van Oss R. The need of polarization monitoring for ozone profile retrieval from backscattered sunlight. J Geophys Res 2002;107:4692.
[38] Stam DM, de Haan JF, Hovenier JW, Stammes P. Degree of linear polarization of light emerging from the cloudless atmosphere in the oxygen A band. J Geophys Res 1999;104:16843.
[39] Jiang Y, Jiang X, Shia R-L, Sander SP, Yung YL. Polarization study of the O_2 A-band and its application to the retrieval of O_2 column abundance. EOS Trans Am Geophys Union 2003;84:255.
[40] Natraj V, Spurr R, Boesch H, Jiang Y, Yung YL. Evaluation of errors from neglecting polarization in the forward modeling of O_2 a band measurements from space, with relevance to the CO_2 column retrieval from polarization-sensitive instruments. JQSRT 2006 in press, doi:10.1016/j.jqsrt.2006.02.073.
[41] Mishchenko MI, Travis LD. Satellite retrieval of aerosol properties over the ocean using polarization as well as intensity of reflected sunlight. J Geophys Res 1997;102:16989.
[42] Deuze JL, Goloub P, Herman M, Marchand A, Perry G, Susana S, et al. Estimate of the aerosol properties over the ocean with POLDER. J Geophys Res 2000;105:15329.
[43] Heintzenberg J, Graf H- F, Charlson RJ, Warneck P. Climate forcing and physico-chemical life cycle of the atmospheric aerosol—why do we need an integrated, interdisciplinary global research programme? Contr Atmos Phys 1996;69:261–71.
[44] Mishchenko MI, Cairns B, Hansen JE, Travis LD, Burg R, Kaufman YJ, et al. Monitoring of aerosol forcing of climate from space: Analysis of measurement requirements. JQSRT 2004;88:149–61.
[45] EPS/METOP System—Single Space Segment—GOME-2 requirements Specification, ESA/EUMETSAT, MO-RS-ESA-GO-0071, 1999: Issue 2.
[46] Crisp D, Atlas RM, Breon F- M, Brown LR, Burrows JP, Ciais P, et al. The orbiting carbon observatory (OCO) mission. Adv Space Res 2004;34:700.
[47] Mishchenko MI. Microphysical approach to polarized radiative transfer: extension to the case of an external observation point. Appl Optics 2003;42:4963–7.
[48] Dahlback A, Stamnes K. A new spherical model for computing the radiation field available for photolysis and heating at twilight. Planet Space Sci 1991;39:671.
[49] Mishchenko M, Hovenier J, Travis L, editors. Light scattering by non-spherical particles. Newyork: Academic Press; 2000.
[50] Hovenier JW, van der Mee C, Domke H. Transfer of polarized light in planetary atmospheres basic concepts and practical methods. Dordrecht: Kluwer Academic Press; 2004.
[51] Mackowski DW, Mishchenko MI. Calculation of the T matrix and the scattering matrix for ensembles of spheres. J Opt Soc Am A 1996;13:2266–78.
[52] Mishchenko MI, Travis LD. Capabilities and limitations of a current FORTRAN implementation of the T-matrix method for randomly oriented, rotationally symmetric scatterers. JQSRT 1998;60:309–24.
[53] Quirantes A. A T-matrix method and computer code for randomly oriented, axially symmetric coated scatterers. JQSRT 2005;92:373–81.
[54] Stamnes K, Thomas G. Radiative transfer in the atmosphere and ocean. Cambridge: Cambridge University Press; 1999.
[55] Anderson E, Bai Z, Bischof C, Demmel J, Dongarra J, Du Croz J, et al. LAPACK user's guide, 2nd Ed. Philadephia: Society for Industrial and Applied Mathematics; 1995.
[56] Stamnes K, Conklin P. A new multilayer discrete ordinate approach to radiative transfer in vertically inhomogeneous atmospheres. JQSRT 1984;31:273.
[57] Wiscombe W. The delta-M method: rapid yet accurate radiative flux calculations for strongly asymmetric phase functions. J Atmos Sci 1977;34:1408–22.

[58] Chami M, Santer R, Dilligeard E. Radiative transfer model for the computation of radiance and polarization in an ocean-atmosphere system: polarization properties of suspended matter for remote sensing. Appl Optics 2001;40:2398–416.
[59] Nakajima T, Tanaka M. Algorithms for radiative intensity calculations in moderately thick atmospheres using a truncation approximation. JQSRT 1988;40:51–69.
[60] Stamnes K, Tsay S-C, Wiscombe W, Laszlo I. DISORT: a general purpose fortran program for discrete-ordinate-method radiative transfer in scattering and emitting media. Documentation of methodology report, available from ftp://climate.gsfc.nasa.gov/wiscombe/Multiple_scatt/, 2000.
[61] Stammes P, Levelt P, de Vries J, Visser H, Kruizinga B, Smorenburg C, et al. Scientific requirements and optical design of the ozone monitoring instrument on EOS-CHEM, In: Proceedings of the SPIE conference on earth observing systems IV. Denver, Colorado, USA, July 1999, vol. SPIE 3750, 221–232.
[64] Cox C, Munk W. Statistics of the sea surface derived from sun glitter. J Mar Res 1954;13:198–227.
[65] Wellemeyer CG, Taylor SL, Seftor CJ, McPeters RD, Barthia PK. A correction for total ozone mapping spectrometer profile shape errors at high latitude. J Geophys Res 1997;102:9029–38.
[66] Spurr R, Christi M. Linearization of the interaction principle: analytic jacobians in the radiant model. JQSRT 2006 in press, doi:10.1016/j.jqsrt.2006.05.001.
[67] Christi MJ, Stephens GL. Retrieving profiles of atmospheric CO_2 in clear sky and in the presence of thin cloud using spectroscopy from the near and thermal infrared: a preliminary case study. J Geophys Res 2004;109:D04316, doi:10.1029/2003JD004058.

Further reading

[62] Caudill TR, Flittner DE, Herman BM, Torres O, McPeters RD. Evaluation of the pseudo-spherical approximation for backscattered ultraviolet radiances and ozone retrieval. J Geophys Res 1997;102:3881–90.
[63] Rozanov AV, Rozanov VV, Burrows JP. Combined differential-integral approach for the radiation field computation in a spherical shell atmosphere: nonlimb geometry. J Geophys Res 2000;105:22937–42.